DOI:
10.1021/acs.molpharmaceut.0c00096

Document Version
Peer reviewed version

Antibiotic-in-cyclodextrin-in-liposomes: formulation development and interactions with model bacterial membranes

Kalliopi-Kelli A. Vandera [($)], Pietro Picconi [($)], Margarita Valero [(&)], Gustavo González-Gaitano [(#)], Arcadia Woods [($)], Nur Masirah M. Zain [($)], Kenneth D. Bruce [($)], Luke A. Clifton [(+)], Maximilian W. A. Skoda [(+)], Khondaker Miraz Rahman [($)], Richard D. Harvey [(¥)]*, Cécile A. Dreiss [($)]*

($) School of Cancer & Pharmaceutical Science, Institute of Pharmaceutical Science, King's College London, Franklin-Wilkins Building, 150 Stamford Street, London, SE1 9NH, UK

(&) Department of Physical Chemistry, University of Salamanca, ES E-37007, Salamanca, Spain

(#) Department of Chemistry, University of Navarra, 31080, Pamplona, Spain

(+) Rutherford Appleton Laboratory, ISIS, 1-27, R3, Harwell Campus, Didcot, UK OX11 0QX

(¥) Department of Pharmaceutical Chemistry, University of Vienna, Althanstraße 14, Vienna, Austria

ABSTRACT: Gram-negative bacteria possess numerous defenses against antibiotics, due to the intrinsic permeability barrier of their outer membrane, explaining the recalcitrance of some common and life-threatening infections. We report the formulation of a new drug, PPA148, which shows promising activity against all Gram-negative bacteria included in the ESKAPEE pathogens. PPA148 was solubilized by inclusion complexation with cyclodextrin followed by encapsulation in liposomes. The complex and liposomal formulation presented increased activity against *E. coli* compared to the pure drug when assessed with the Kirby Bauer assay. The novel formulation containing 1 μg PPA148 reached similar efficacy levels equivalent to those of 30 μg pure rifampicin. A range of biophysical techniques was used to explore the mechanism of drug uptake. Langmuir trough (LT) and neutron reflectivity (NR) techniques were employed to monitor the interaction between the drug and the formulation with model membranes. We found evidence for fluidosome fusion with the model Gram-negative outer membrane and for cyclodextrins acting as inner membrane permeation enhancers without presenting intrinsic antimicrobial activity. An antibiotic-in-cyclodextrin-in-liposomes (ACL) formulation was developed, which targets both the bacterial OM and IM, and offers promise as a means to breach the Gram-negative cell envelope.

KEYWORDS: Antimicrobial resistance, Antibiotic formulation, Membrane fusion, Langmuir monolayers, Neutron reflectivity, Asymmetric bilayer

ABBREVIATIONS: OM: Outer membrane, IM: Inner membrane, LPS: Lipopolysaccharide, PBD: pyrrolobenzodiazepine, MIC: Minimum inhibitory concentration, CD: Cyclodextrin, RAMEB: Randomly methylated cyclodextrin, HPβCD: Hydroxy propyl β cyclodextrin, DIMEB: heptakis (2,6-di-O-methyl)-β-cyclodextrin, *E. coli*: *Escherichia coli* , DLS: Dynamic light scattering, DCR: Derived Count Rate, LT: Langmuir trough, LB: Langmuir-Blodget, LS: Langmuir-Schaefer, NR: Neutron reflectivity, ACL: Antibiotic in cyclodextrin in liposomes, Tm: Phase transition temperature

1 INTRODUCTION

The Gram-negative bacterial cell envelope consists of a double-membrane and peptidoglycan layer, which provide intrinsic protection against the uptake of antibiotics, due to the presence of lipopolysaccharide (LPS) in the outer membrane (OM) and envelope-spanning efflux pumps (1–4). Inter-species horizontal gene transfer between Gram-negatives has also led to the rapid proliferation of multi- or pan-drug resistance amongst these bacteria, and led to their being listed as a critical priority for antimicrobials research by WHO (1,5). This has attracted a great deal of interest in research to develop novel classes and variants of antibiotics (6,7), the activity of which may be augmented by formulation approaches aimed at increasing OM permeability and inhibiting efflux (8).

This study focuses on a novel antimicrobial agent, PPA148, belonging to the pyrrolobenzodiazepine (PBD) group of anticancer and antimicrobial drugs (Figure 1 and Supporting Information Table S1). PBDs are naturally occurring sequence-specific DNA minor groove binding agents produced by Streptomyces bacteria which have been evaluated as potential

antibacterial agents in recent years (9–11). PBDs have shown promising activity against Gram-negative bacteria amongst the so-called ESKAPEEs, a group of pathogens of major clinical interest, in particular *Acinetobacter baumannii* and *Klebsiella Pneumoniae* (with MICs < 2 μg/ml in each case) (12). PPA148 is a large, non-ionic, poorly water-soluble drug, whose bactericidal activity is attributed to the inhibition of bacterial DNA gyrase, thus disrupting chromosomal replication and leading to cell death. Microbiological evaluation of PPA148 against *Pseudomonas aeruginosa* showed that the compound was most effective in the presence of efflux pump inhibitors or membrane permeabilizers, highlighting that PPA148 may be subject to efflux and thus exhibits low permeability into these bacterial cells (12).

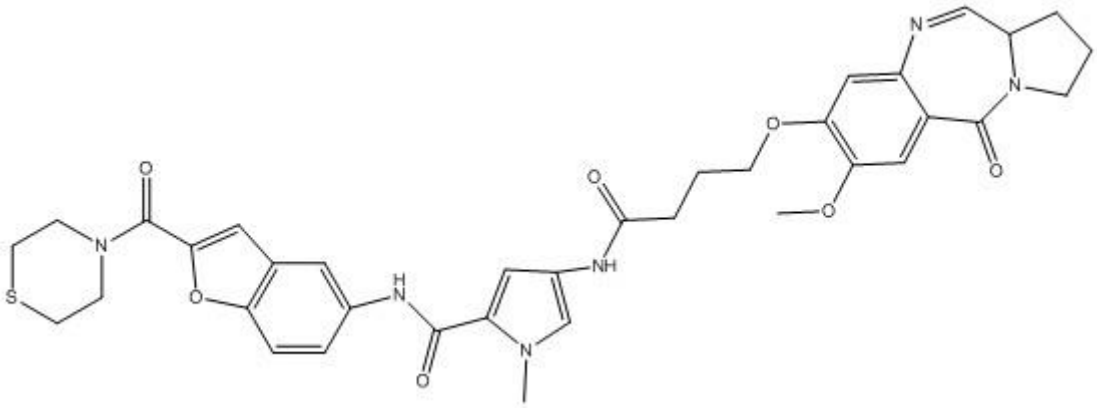

Figure 1. Chemical structure of PPA148 (MW = 698.2 g/mol). ChemDraw software was used to estimate the physicochemical properties, which address a highly hydrophobic molecule with logP of 0.76 and logS of -7.5.

Improving the solubility of PP148 is a necessary first step towards developing a formulation for pulmonary delivery to increase its efficacy. For this purpose, we have investigated the use of cyclodextrins, since they have been used widely as solubilizing agents and can encapsulate a wide range of lipophilic molecules through the formation of inclusion complexes (13). β-cyclodextrin

and its derivatives in particular (such as hydroxypropyl- and randomly methylated- βCD) have been reported not only to enhance the solubility of poorly soluble drugs but also to increase their internalization into cells and improve their biological activity against Gram-negative bacteria (14–16). For instance, the stability and bactericidal action of antibiotics such as meropenem have been enhanced by inclusion complex formation with native βCD (15). Complexation of rifampicin, tobramycin and gentamicin with hydroxypropyl- βCD (HPβCD) and randomly methylated βCD (RAMEB) were shown to improve the drugs' biological activity and to eliminate toxicity (16). EMA has reported that HPβCD and RAMEB increase the nasal and pulmonary drug permeability and are safe for nasal administration in concentrations below 10% (17). Drug/CD complexes are in dynamic equilibrium with free drug and free CD molecules and dissociation might occur after administration to the lungs, which affects drug bioavailability. Dissociation of moderately weak inclusion complexes (binding constant below 10^4 M^{-1}) might be a result of simple dissolution at the site of administration and/or of competitive inclusion effects due to higher affinity of CD towards proteins or lung surfactant, such as cholesterol (18,19). In order to reduce this risk of dissociation, liposomes were used as a carrier of the PPA148/CD complex. The resultant antibiotic-in-cyclodextrin-in-liposome (ACL) formulation (20) combines the properties of cyclodextrins as solubilizing agents and DPPC/DMPG [18:1] fluidosomes as liposomal carriers with the potential to fuse with the Gram-negative OM and thus improve drug permeability and circumvent efflux mechanisms (21,22). Fluidosomes are unlikely to fuse into human pulmonary cells whereas they can fuse into bacterial membranes (23), which could provide specificity to the proposed ACL formulation.

Since both cyclodextrins and fluidosomes have the potential individually to enhance the antimicrobial efficacy of the ACL formulation, the activities of the different components were

compared with that of pure PPA148, and the possible physical envelope-breaching mechanisms underlying ACL action were explored using a range of interfacial biophysical techniques. These included an assessment of membrane binding of various formulation components, using adsorption isotherms on lipid monolayers at the air/liquid interface, and neutron reflectivity on a supported asymmetric Gram-negative model OM to gain molecular-level structural insight into its interaction with fluidosomes, and further to determine the feasibility of a putative fusion mechanism. The biophysical investigation was carried out alongside microbiological assays, which compared the efficacy of PPA148 with that of rifampicin.

While there have been reports of antibiotics solubilized by either inclusion complexes with CDs, or encapsulated in liposomes, we are not aware of any published work on antibiotics formulated in ACL. This study constitutes the first formulation approach for the antimicrobial agent PPA148 as well as the first report of the biophysical characterization and efficacy assessment of the novel ACL formulation applied to PPA148.

2 MATERIALS

Drugs: PPA148 (Mw = 698.25 g/mol, with an estimated clogP of 2.09 and logP of 0.76) was custom synthesized in the Institute of Pharmacy at King's College London (12,24). Rifampicin (purity: 97.1%) was purchased form Sigma-Aldrich, UK. Lipids: Phospholipids 1,2-dipalmitoyl-*sn*-glycero-3-phosphocholine (DPPC, 16:0 PC), 1,2-dipalmitoyl-d_{62}-*sn*-glycero-3-phosphocholine (d_{62}DPPC, 16:0 PC-d_{62}) and 1,2-dimyristoyl-*sn*-glycero-3-phosphoglycerol, sodium salt (DMPG, 14:0 PG) were supplied by Avanti Polar Lipids (Alabama, USA). Rc LPS from *Escherichia coli* J5 (purity: protein 1.4%, nucleic acid 0.340%, phosphate 7.3%, Kdo 5.9%), Ra LPS from *E. coli* EH100 and Re Lipid A from *Salmonella minnesota* R595 containing ≤0.3% proteins were all

obtained from Sigma-Aldrich, UK. and were used without further purification. Cyclodextrins: Hydroxypropyl- β-cyclodextrin (HPβCD), randomly methylated β-cyclodextrin (RAMEB) and heptakis (2,6-di-O-methyl)-β-cyclodextrin (DIMEB) were purchased from Sigma-Aldrich, UK. Solvents: Chloroform ($CHCl_3$), dimethyl sulfoxide (DMSO), deuterium oxide (D_2O), %) were purchased from Sigma-Aldrich, UK. Ultrapure water with a specific resistivity of 18.2 MΩ·cm was produced by a Purelab Ultra machine from ELGA Process Water (Marlow, UK). Salts for buffers: magnesium sulfate ($MgSO_4$) was purchased from Sigma-Aldrich, UK, and used at the drug extraction process. Sodium chloride (NaCl), and magnesium chloride ($MgCl_2$) were supplied by Sigma-Aldrich, UK, and were used in the monolayer studies. HEPES (>=99.5%) and calcium chloride ($CaCl_2$) were purchased from Sigma-Aldrich, UK, and were used for liposome preparation and neutron reflectivity measurements. Microbiology: Blank, rifampicin (30 μg) and vancomycin (30 μg) susceptibility disks, agar powder and Muller Hinton broth for microbiology were purchased from Oxoid (UK). Escherichia coli bacteria DH5α were obtained from Invitrogen Life Science Technology (Thermo Fisher Scientific, UK).

3 METHODS

3.1 Formulation development

3.1.1 Aggregation of PPA148 by Light Scattering and turbidimetry

The aggregation of the drug and its solubility in aqueous media with and without cyclodextrins, were evaluated using both light scattering and turbidimetry. A stock solution of PPA148 (5 mM) in DCM was used to produce a range of concentrations (0 - 160 μg/ml) in water, and in the presence and absence of 1% HPβCD, by evaporation of DCM. Samples were left under mild stirring for 7 days. Dynamic light scattering (DLS) measurements were performed at 25°C on a Malvern

Zetasizer (Nano-ZS, Malvern Instruments, UK) with a laser of wavelength 623.8 nm and backscatter detection angle of 173°. The derived count rate (DCR) was recorded and its normalized form plotted against drug concentration. The same samples were also assessed by turbidimetry, using a UV/Vis spectrophotometer (Lamda 2, Perkin Elmer, UK) at a wavelength of 620 nm.

3.1.2 Thermodynamic solubility of PPA148 by UV spectroscopy

An excess of PPA148 (1 mg) was added to deionized water and 20 mM HEPES, 2 mM $CaCl_2$, 145 mM NaCl (pH =7.2) buffer (1 mL) in the presence and absence of 1% HPβCD and 1% RAMEB. The samples were kept under mild stirring (290 rpm) for 7 days. After incubation, samples were centrifuged (5 min at 10,000 rpm) and the supernatant was freeze-dried overnight and resuspended in ethanol/water (volume ratio of 4:1). The saturated concentration was assayed by UV/Vis spectroscopy. The UV spectrum of PPA148 was recorded on a Lamda 2 spectrophotometer (Perkin Elmer, UK), at 25˚C using a quartz cuvette (Hellma 114-QS). Absorbance spectra were recorded between 200-550 nm, using a slit width of 2 nm and scan speed of 60 nm/min.

The linearity of this method was determined by analyzing the solutions of PA148 in the range of 2-200 µg/mL. For quantification purposes, the Limits of Detection (LOD) and Quantification (LOQ) were established by regression analysis of the linear region of the calibration curve. Both values were calculated using the standard error of the mean (se) and slope (S) taken from the regression line, using the following:

$$LOD = \frac{3.3 \times se}{S} \quad (1)$$

$$LOQ = \frac{10 \times se}{S} \quad (2)$$

3.1.3 Quantification of drug/cyclodextrin binding constant by fluorescence spectroscopy

The binding constant of PPA148 for cyclodextrins (HPβCD and RAMEB) was measured by fluorescence spectroscopy, following established methods (25). Specific volumes of either PPA148 in DCM, or rifampicin in ethanol were transferred into separate vials and the solvent evaporated. Two types of modified β-cyclodextrins were used: HPβCD and RAMEB and their solutions (0 - 30%) in HEPES (20 mM) buffered saline, pH 7.2 were then added to achieve a final drug concentration of 10 µg/mL. The samples were left under mild stirring overnight.

The fluorescence intensity from PPA148 was measured with a Luminescence spectrometer LS 50 B (Perkin Elmer, UK), and was conducted with an excitation wavelength of 300 nm, and an emission wavelength scan range of 340-530 nm, with emission/excitation slit widths of 5 nm. The fluorescence intensity of the drug was plotted as a function of concentration. The binding constant (K_2) of a 1:2 drug/CD complex, was determined by fitting the data to the following equation (26):

$$I = \frac{I_0 + I_1\, k_1[CD] + I_2\, k_1 k_2 [CD]^2}{1 + k_1[CD] + k_1 k_2 [CD]^2} \qquad (3)$$

$$K_2 = k_1 \times k_2 \qquad (4)$$

where I_0, I_1 and I_2 are the experimental fluorescence intensity from the drug in the absence of cyclodextrin, at the first binding site and the second binding site with the drug, respectively. The I_2 value corresponds to the fluorescence value at the plateau of the curve. For a 1:2 drug/CD complex, the binding constants of the drug with the first and second CD unit, i.e. k_1 *and* k_2 respectively, were determined by fitting the data with equation 3. The binding constant of a 1:2 drug/CD complex is given by equation 4.

A non-linear least squares method was used to fit the experimental results to Equation 3. The differences between the calculated fluorescence and the experimentally derived data were minimized by varying the values of the binding constant (the iterative approach of Nelder–Mead) using the Microsoft Excel Solver function (27). The binding constant of a 1:2 complex is presented as the mean of three batches.

3.1.4 Stoichiometry of the drug/DIMEB complex by ^{1}H NMR: Job's Plot

The stoichiometry of the drug/DIMEB complex was studied by liquid state 1-dimensional (1D) proton (^{1}H) NMR spectroscopy. 1H NMR spectroscopy was carried out on an AscendTM 400 MHz spectrometer equipped with a SampleXpress autosampler system (Bruker, UK). The parameters included sweep width of 8012.82 Hz, acquisition time of 4.09 s and 16 scans and were collected with a zg30 pulse program.

The applied method is known as the continuous method variation or Job's plot (28). DIMEB, which is methylated in two positions of each glucose unit, was used as it provides a high resolution spectrum from which all the protons can be assigned, unlike RAMEB and HPβCD, which are randomly substituted and therefore lead to spectra with broad peaks (29). Equimolar solutions (1mM) of PPA148 and DIMEB in D_2O were prepared and mixed in varying volume fractions whilst keeping the total concentration constant (1 mM). PPA148 and DIMEB solutions were mixed in volume fractions ranging from 0 to 1 mL with an increment of 0.1 mL. The inclusion of PPA148 into the DIMEB cavity is detected by changes in the chemical shift observed with selected protons of the cyclodextrin. The resonances of the DIMEB interior hydrogens, i.e. in positions 3 (H3) and 5 (H5), were observed as a triplet at 3.90, 3.92 and 3.94 ppm and as a doublet at 3.84 and 3.86

ppm, respectively. The chemical shift of the exterior proton in position 1 (H1) was presented as a doublet at 5.19 and 5.18 ppm. (30) (31).

The stoichiometry of the complex was obtained by normalizing the variations of the chemical shifts of the host by its mole fraction (X_{CD}) and plotting them against cyclodextrin mole fraction (X_{CD}) (32). The shift of the DIMEB hydrogen resonance depends on the mole fraction of pure drug, pure DIMEB and drug/DIMEB complexes. A 1:1 complex presents a maximum signal at 0.5 CD mole fraction.

3.1.5 Preparation of drug-cyclodextrin inclusion complexes

A 1:2 complex of drug and RAMEB was used for its encapsulation into liposomes. Drug and cyclodextrin were mixed in a 1:2 molar ratio in HEPES buffered saline at pH 7.2. The mixture was continuously stirred (190 rpm) for 24 hours in order to ensure equilibrium and complex formation.

3.1.6 ACL preparation

Fluidosomes consisting of DPPC/DMPG in an 18:1 molar ratio were prepared by the thin film solvation method (33). The mixture of lipids (20 mg total) was dissolved in 1 mL of chloroform in a round-bottomed flask and bath sonicated (Fisherbrand®, FB11203, Fisher Scientific, UK) at 25°C for approximately 1 min to achieve a visibly clear solution. The solvent was evaporated using a rotary evaporator (Rotavapor® RII, Büchi, Switzerland) attached to a vacuum pump (KNF Lab, UK). The temperature of the water bath was set to 40°C and the rotation speed to approximately 190 rpm. The resulting thin lipid film was kept under reduced pressure in a Pyrex vacuum desiccator for 12 h to remove any traces of organic solvent. The lipid film was then solvated by adding 4 mL of 20 mM HEPES buffered saline pH 7.2 (145 mM NaCl and 10 mM $CaCl_2$) containing the previously prepared inclusion complexes under vigorous stirring and bath

sonication (Fisherbrand®, FB11203, Fisher Scientific, UK) at 40°C to facilitate vesicle formation. The lipid suspension was dipped into an ice bath (4°C) for 1 min and then placed in the water bath (40°C) for another minute. This temperature changing sequence was repeated 5 times followed by a 1 h annealing period at 4°C before using them for size reduction.

Size reduction of ACLs was carried out by extrusion, to produce homogeneous dispersions of unilamellar vesicles. A 1 mL ACL dispersion was loaded into a gas-tight syringe in a mini-extruder (Avanti Polar Lipids, AL, USA) thermostatically heated to 55°C and manually extruded through a 0.1 μm pore polycarbonate membrane 11 times. The extruded ACLs were kept at 4°C and were extruded again under the same experimental set up after 12 hours. The double extruded ACLs were stored at 4°C before measuring their size using PCS. All samples were prepared and measured in triplicate.

Size exclusion chromatography was used to separate the liposomes from the unentrapped drug/CD complexes. A Sephadex™ G-25 PD-10 column (GE Healthcare, UK) was equilibrated with 15 mL of 20 mM HEPES buffered saline, pH 7.2. Each liposome mixture (1 mL) was allowed to penetrate the gel entirely and the eluted volume was discarded. Then, aliquots of HEPES buffered saline (1 mL) were added to the column sequentially (8 times) to elute various fractions which were collected separately. Each fraction was characterized for its hydrodynamic diameter, derived count rate, lipid and drug concentration to determine which aliquot contained the majority of the loaded liposomes. The determination of lipid concentration was achieved using the colorimetric Stewart assay (34).

Drug quantification was carried out using UV/Vis spectroscopy to determine the encapsulation efficiency (EE) and the drug loading (DL) of liposomes. PPA148 was extracted from all 8 aliquots

collected after size exclusion chromatography. Each aliquot was washed with DCM and the organic phase was collected, dried with magnesium sulfate ($MgSO_4$) and evaporated under vacuum (Rotavapor® RII, Büchi®, Switzerland and KNF Lab vacuum pump, UK). The resulting dry sample was re-suspended in ethanol/water (80:20) and the unknown drug concentration was calculated by interpolating from a linear calibration curve, which was determined under the same experimental conditions. The area under the curve (AUC) of all samples was used for drug quantification (35) and calculated using GraphPad Prism 7.03 software (GraphPad software Inc., USA). The test samples were run in quadruplet replicates and the calibration curve samples per concentration were run in triplicate. The Encapsulation Efficiency (EE) and Drug Loading (DL) were calculated using the following equations:

$$EE\ (\%) = \frac{C_T - C_u}{C_T} \times 100\% \qquad (5)$$

$$DL\ (\%) = \frac{C_T - C_u}{C_L + C_T - C_u} \times 100\% \qquad (6)$$

where C_u is the un-entrapped drug concentration, C_L and C_T are the concentration of lipids and drug added into the liposome system, respectively.

3.1.7 Kirby Bauer assay to assess the efficacy of PPA148-in-RAMEB-in-fluidosomes

The Kirby Bauer method, also known as the disk diffusion assay, is commonly used for testing the susceptibility of bacteria to drugs and chemicals (36,37). E. coli was cultured on a Mueller-Hinton (MH) agar (21 g/L MH broth and 17 g/L agar) from a gel-bead for 24 h at 37˚C. Bacterial colonies were transferred in MH broth until the optical density (OD) of the bacterial suspension reached 1 (~8×108 cells/mL) at 600 nm. The OD was measured using a single beam JENWAY 6300 Visible Spectrophotometer (Staffordshire, UK) with resolution of 1 nm and spectral bandwidth of 8 nm.

To stop bacterial growth, 1 mL of the suspension was centrifuged at 10,000G for 5 min and the bacterial pellets were re-dispersed in sterile physiological saline (0.9% NaCl). An aliquot of this suspension (100 µL) was spread onto an MH agar plate, and filter disks impregnated with antibiotic were placed on top. The plates were incubated for 24 h at 37˚C, after which the diameter of the inhibition zones surrounding the antibiotic disks, was measured.

Commercially available disks for rifampicin (30 µg) and vancomycin (30 µg) were used as positive and negative controls respectively, based on their differing abilities to inhibit Gram-negative bacterial growth. However, the filter disk for the novel antibiotic (PPA148 1 µg) as well as for the complex and ACF, were prepared in-house. All stock solutions (PPA148 5 mM in DCM, 1:2 complex (0.5 mg/mL), 5% RAMEB and ACF 0.5 mg/ml) were sterilized using a UV lamp (Spectroline®, ENF-24C/FE, Spectronics corporation, Westbury, New York, USA) at 254 nm (ultraviolet germicidal irradiation). A volume equivalent to PPA148 1 µg was placed on the paper disk plate, absorbed and evaporated under reduced pressure. To validate the preparation method of the in-house disks, disks containing 30 µg of rifampicin were prepared using the same method and the results were compared to those of the commercially available disks. All samples were prepared and tested 10 times.

3.2 Mechanistic investigation

3.2.1 Gibbs isotherms of drug-monolayer interactions

Gibbs isotherms were used to assess the interaction of PPA148, rifampicin, cyclodextrins and fluidosomes with biomimetic lipid monolayers (DPPC/DPPG (3:1), Lipid A and J5 LPS). DPPC was chosen instead of PE lipids, which are one of the predominant lipids in bacterial cell envelope

(38,39), to avoid artefacts arising from the tendency of PE to form negatively curved interfaces (40,41). The mixture DPPC/DPPG keeps the interface planar.

A 50 mm diameter perfluoroalkoxy (PFA) petri dish (Saint-Gobain Performance Plastics) with a 20 mL capacity was placed over a magnetic stirring plate and filled with a filtered 1 mM $MgCl_2$ solution or 20 mM HEPES buffered saline containing 2 mM $CaCl_2$ (pH 7.2) through a 0.45 μm Minisart® filter, under mild stirring. A Wilhelmy plate (Whatman, grade 1, chromatographic paper) connected to a calibrated NIMA PS4 (0-240 mN/m range, 0.1 mN/m resolution) pressure microbalance was submerged into the subphase. A syringe containing 100 μL PPA148 solution in DMSO or one of the other samples in water was placed with its hypodermic needle (gauge 25G, BD biosciences UK, Oxford, UK) penetrating into the subphase. Any alteration in surface pressure produced upon injection of the sample, as molecules adsorbed or desorbed at the air/liquid interface were recorded by the microbalance. Prior to subphase injection, a lipid solution in chloroform (1 mg/mL) was spread dropwise at the air/water interface until the surface pressure reached 30-35 mN/m (the lateral pressure in biomembranes) (42), while stirring the subphase with a 4.5×15 mm magnetic stirrer bar set at its minimum speed to avoid variation of pressure greater than 0.2 mN/m. A period of 40 to 60 min was allowed for the solvent to evaporate and for the monolayer to reach equilibrium (stabilization of the surface pressure, $\Pi_{initial}$). Drug solution (0.1 mL) was then injected below the lipid monolayer to produce a final concentration in the trough of 20 μg/mL. Changes in surface pressure were recorded until a new pseudo-plateau was reached (Π_{max}).

The rate of change in surface pressure ($\Delta\Pi$) was plotted against time and the binding isotherms produced were fitted with a sigmoidal 3-parameter Hill plot using GraphPad, Prism 7 (GraphPad Software, CA, USA) to obtain the kinetic parameters as follows:

$$y = \frac{\Delta\Pi_{max} x^h}{t_{50\%}^h + x^h} \qquad (7)$$

where $\Delta\Pi_{max}$is the maximum difference in surface pressure ($\Delta\Pi_{max} = \Pi_{max} - \Pi_{initial}$), h is the hill coefficient, and $t_{50\%}$ is the time needed to achieve half $\Delta\Pi_{max}$. The Hill coefficient describes the overall growth or decrease rate of the curve and is a measure of how quickly the curve moves from the lower asymptote to the upper asymptote or the opposite. Large h (steep curve) describes a fast change in surface pressure and high affinity of the drug towards the air/liquid interface. All samples were prepared and tested in triplicate.

3.2.2 Interaction of fluidosomes with a model Gram-negative outer membrane assessed by Neutron reflectivity

3.2.3 Solid-supported asymmetric DPPC and LPS bilayer (model OM) deposition

The lipid components of model Gram-negative bacterial membranes were deposited onto the piranha-cleaned polished oxidized surface of 50×80×20 mm single silicon crystals (Crystran, Poole, UK.), using a Langmuir trough (KSV-NIMA, Biolin Scientific, Finland). The Langmuir-Blodget (LB) technique was used to deposit the inner leaflet of the membrane (d_{62}DPPC) on the 50×80 mm polished surface of the crystal, and Langmuir-Schaefer (LS) deposition used for the outer leaflet of the membrane (hydrogenous *E. coli* EH100 LPS or hLPS), following the method of Clifton *et al*. (43,44).

Three isotherm cycles were conducted prior to deposition to examine the stability of the monolayers (see Supporting Information, Figure S9). For the LB deposition, the silicon block was submerged into the ultrapure non-buffered water subphase, which contained 5 mM $CaCl_2$ and was cooled to 10°C to improve interfacial coverage. A solution of d_{62}DPPC in chloroform was

deposited dropwise on the subphase surface and compressed slowly to a constant surface pressure of 38 mN/m. The silicon crystal was lifted through the air-water interface at a speed of 4 mm/min while keeping the surface pressure constant at 38 mN/m. The silicon block was therefore covered with a homogeneous d-DPPC monolayer, having the headgroup towards the silicon block and the hydrophobic tails facing the environment.

The Langmuir trough was then cleaned and the air-liquid interfacial monolayer of hLPS (2.5 mg/mL) was deposited (from 60% chloroform, 39% methanol and 1% water v/v) on to the same composition clean non-buffered interface, cooled at 10°C, with a surface pressure of 38 mN/m. The LS deposition was achieved by securing the previously covered silicon block into a holder above and parallel with the interface with the previously deposited DPPC acyl chains pointing downward, toward the interface. The silicon block was lowered at a speed of 3 mm/min through the interface in order to allow the lipid monolayer on the block to match the LPS monolayer on the subphase via the hydrophobic chains, producing a solid supported asymmetric bilayer (model OM) (43). The block was then allowed to continue moving downwards until the bottom of the trough was reached where a customized PTFE sample cell was placed. The sample cell and silicon block were secured in a custom-made metal holder to ensure the bilayer was fully contained and sealed inside the small water chamber of the sample cell, whose total volume was 3 mL.

3.2.4 Neutron reflectometry measurements

Specular neutron reflectometry (NR) measurements were conducted using the INTER reflectometer at the ISIS neutron source, Rutherford Appleton Laboratory (STFC, Oxfordshire, UK), using neutron wavelengths from 1.5 to 16 Å. The reflected intensity was measured at two incident angles of 0.7° and 2.3° as a function of the momentum transfer Q ($Q = \frac{4\pi \sin\theta}{\lambda}$, where λ

is the wavelength and θ is the incident angle). The purpose-built flow cell of the silicon-liquid interface (described above) was placed on an anti-vibration sample stage and the inlet of the cell was connected to a L7100 HPLC pump (Merck, Hitachi, Germany).

One solid-supported model OM was used in this experiment and NR was carried out at 38°C under two different conditions, i.e. before and after the challenge with liposomes. Once the data collection was completed for the unchallenged model OM, fluidosomes (0.1 mg/mL in 20 mM HEPES buffered saline containing 2 mM $CaCl_2$ pH 7.2) were injected into the sample cell via the HPLC pump at a 1.5mL/min flow rate and allowed to incubate for 1 h. The excess fluidosomes were flushed out of the cell chamber at a rate of 1.5mL/min before data acquisition, in order to measure the possible structural changes caused by their interaction with the model OM.

Both experimental treatments of the model OM were examined under three different isotopic contrast conditions, i.e. 100% H_2O, 100% D_2O and silicon matched water or SMW (38% D_2O, 62% H_2O), to highlight the different components of the bilayer structure. All isotopic solutions contained 20 mM HEPES, 145 mM NaCl and 5mM $CaCl_2$ to maintain the asymmetry of the model OM. The HPLC pump facilitated automated exchange of the different contrast solvents within the cell (3 mL) at a flow rate of 1.5 mL/min.

3.2.5 NR data fitting and Statistical analysis

RaScal software was used to fit the experimental data on Born and Wolf's optical matrix formalism to convert the raw reflectivity data into a real space description of the scattering length density across the interface (45,46). The interface is described as a series of slabs, each one representing different compartments of the solid-supported model OM, i.e. the silicon oxide layer of the crystal, inner headgroup, inner tails, outer tails and outer headgroup layer. Bayesian Markov Chain Monte

Carlo (MCMC) statistics with 95% confidence interval were applied to estimate the parameters most likely to produce the experimental reflectivity data observed given the already known layered model (47,48). The parameters of interest were the scattering length density (SLD), thickness, roughness and hydration state of each layer. In addition to the model parameters, the backgrounds, scale factors and instrument resolutions were also fitted. The MCMC was carried out for thousands of iterations and Chi squared (X^2) was used to adjust the fit of the parameters by reducing the difference between the known layered model and the experimental reflectivity data. For all sets of data, the simplest (least number of layers) model was selected based on the overall chi-squared. Due to the complexity of the five-layered model, a skewed data distribution was assumed and thus the lower and upper values of each parameter were presented instead of a standard deviation.

The three contrasts used for each experimental treatment produced three reflectivity profiles which were simultaneously fitted. The difference in SLD of the d_{62}DPPC and hLPS tails in the three solvent contrasts was used to determine the volume fraction of the water in each leaflet of the model OM. In the tail region of d_{62}DPPC and hLPS, neither lipid tails possess labile hydrogens and, therefore, do not undergo changes in SLD (ρ). The calculated volume fraction of water and the SLD experimental values of the of d_{62}DPPC tails, LPS tails were measured, the volume fraction of the DPPC tails can be calculated as described in detail by Clifton *et al*.(2013) (43).

The asymmetry of the model OM was examined by calculating the volume fraction of water and d_{62}DPPC tails (PC tails) in each leaflet as described in Clifton *et al*. (2015) (49).

4 RESULTS

4.1 Aggregation and thermodynamic solubility of the drug

Solubility studies with UV-Vis spectroscopy revealed that for concentrations between 1-15 μg/mL, the absorbance of PPA148 in water is proportional to its concentration, but it deviates at higher concentrations (see Supporting Information, Figure S1), suggesting the presence of molecular aggregates. Figure 2 presents the changes in normalized derived count rate (nDCR) against drug concentration in water at 25°C; the sharp increase in nDCR reflects the onset of critical aggregation (50), which occurs around 20 μg/mL. DLS measurements reveal aggregates of average size 1-18 μm and a high polydispersity index (0.7) (see Supporting Information, Figure S2). A similar aggregation concentration value was obtained with turbidity measurements using UV/Vis spectroscopy at 620 nm (Figure 2, Table 1). The scattering of light upon increasing drug concentration in water presented a more variable profile, which is an indication of PPA148's very low solubility and high propensity to aggregate in water. Precipitation of the drug in water was visually observed at concentrations higher than ~30 μg/mL. In the presence of HPβCD, the aggregation limit is shifted to higher concentrations (ca. 50 μg/mL), confirming the capacity of the cyclodextrins to solubilize the drug, likely through inclusion complex formation (Figure 2).

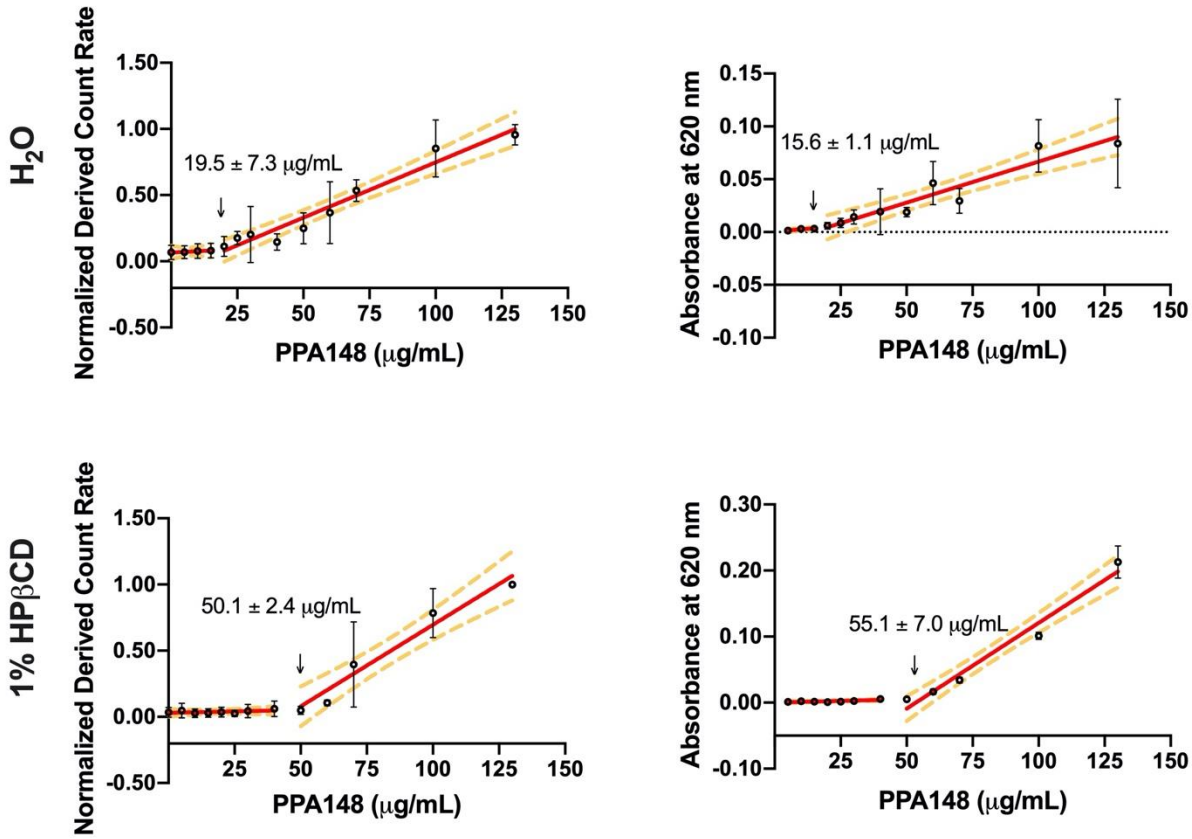

Figure 2. Turbidimetric assay: Effect of 1% HPβCD (7 mM) concentration on the aggregation of PPA148 in ultra-pure water (18.2 MΩ·cm) at 25°C using dynamic light scattering (right) and UV/Vis spectroscopy (left). The data are presented as normalized derived count rate and absorbance at 620 nm against PPA148 concentration in water (top) and 1% HPβCD (bottom). The red line is the linear regression fit and the orange lines are the 95% confidence intervals. The intersection of the two linear models provides the aggregation concentration.

The thermodynamic solubility (S_0) of PPA148 was investigated in water and HEPES buffer saline pH 7.2 by UV spectroscopy at the maximum absorbance of PPA148. RAMEB and HPβCD were shown to solubilize PPA148 up to approximately 50 µg/mL in HEPES buffered saline pH 7.2 (Figure 2, Table 1).

Table 1. Solubility and aggregation of PPA148 in the presence and absence of 1% HPβCD (7 mM) and/or 1% RAMEB (8 mM) (n=3).

Solvent	Solubility (µg/mL)	Aggregation concentration (µg/mL)	
	Thermodynamic solubility	Turbidimetric assay (PCS)	Turbidimetric assay (UV)
H_2O	30.3 ± 1.8	18.1 ± 4.7	16.3 ± 11.1
HEPES	55.8 ± 15.9	-	-
HPβCD/H2O	-	51.1 ± 2.6	53.9 ± 12.1
RAMEB/HEPES	90.5 ± 4.4	-	-

4.2 Quantification of drug/cyclodextrin binding constant by fluorescence spectroscopy

The interaction of PPA148 with cyclodextrins and the binding constant of the inclusion complex was investigated using fluorescence spectroscopy. Shifts in the fluorescence drug peak at 422 nm for PPA148 are due to inclusion complex formation because the drug is transferred from the polar aqueous phase to the less polar CD cavity. The addition of increasing concentrations of cyclodextrin (either RAMEB or HPβCD) from 0 to 30 % w/v (0-171 mM for HPβCD and 0-225 mM for RAMEB) to a fixed concentration of 10 µg/mL PPA148 produces a hyperchromic effect, reflecting changes in the environment, in which the whole or part of the drug is included in the cavity of HPβCD or RAMEB. The experimental data were fitted using Equation 3 (Figure 3A), which describes the formation of a 1:2 drug/CD complex.

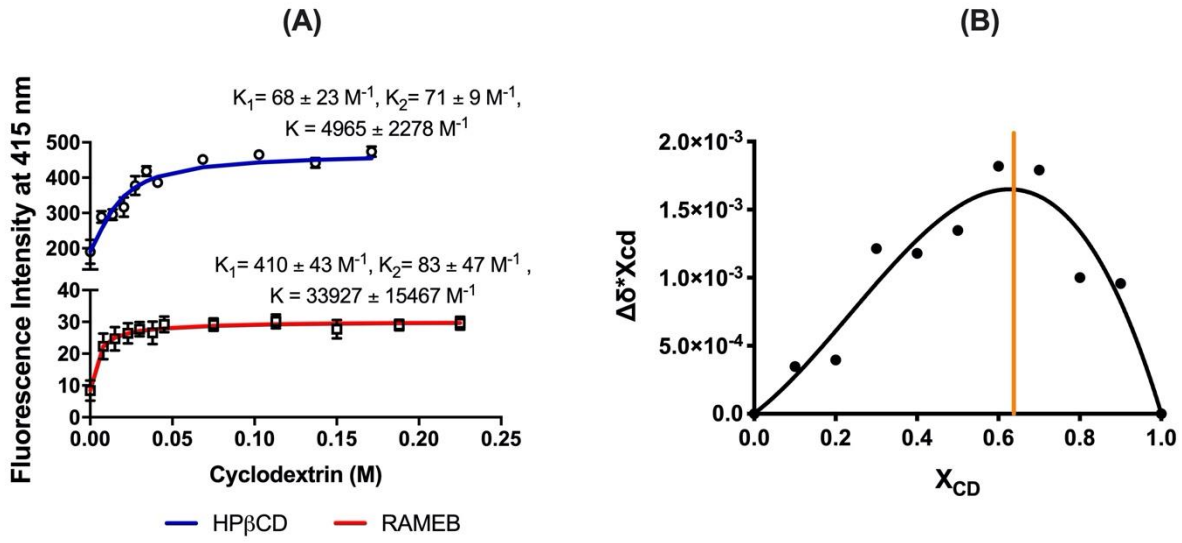

Figure 3. (A) Binding constant assay of the 1:2 complex between PPA148 (10 μg/mL) with RAMEB and HPβCD using fluorescence spectroscopy at 25°C (n = 3). (B) Job's plot showing the 1:2 stoichiometry of the PPA148/DIMEB complex in D_2O using ^{1}HNMR spectroscopy.

4.3 Stoichiometry of the drug/DIMEB complex by ^{1}H NMR: Job's Plot

DIMEB was used as a model of methylated β-cyclodextrin to measure the stoichiometry of the inclusion complex between PPA148 and methylated β-cyclodextrins. DIMEB is methylated in two specific sites on the CD molecule and thus gives narrow peaks in the ^{1}H NMR spectrum compared to the randomly methylated and hydroxy-propylated β-cyclodextrins used in the formulation (RAMEB and HPβCD). PPA148 was used below its solubility limit (20 μg/mL, or 0.03 mM). As a result, the spectra obtained were quite noisy, due to the low concentration, but the chemical shifts of the hydrogen at position 5 (H5) were clearly detected (see Supporting Information, Figure S3) and show a skewed Job's plot with a maximum around X_{CD}=0.6 (Figure 3B), reflecting a 1:2 PPA148/DIMEB complex, namely, the drug complexes with two cyclodextrins in two different positions.

4.4 Preparation of drug-cyclodextrin inclusion complexes

Based on the higher affinity of PPA148 for RAMEB (Figure 3A), this cyclodextrin was selected for encapsulation in fluidosomes to evaluate the full formulation. The elution profile of loaded fluidosomes (DPPC/DMPG in 18/1 molar ratio) is presented in Figure 4A. The derived count rate (DCR) profile showed that the majority of fluidosomes eluted in the third fraction (Figure 4A), with a size of 129 ± 1 nm (see Supporting Information, Figure S4). The difference between the size of the empty (128 ± 2 nm) and PPA148/RAMEB encapsulated fluidosomes was not statistically significant ($p=0.25$).

A Stewart assay was used to quantify the DPPC content in the eluted fractions of fluidosomes because it accounts for 95% of lipids in the mixture (DPPC/DMPG [18/1]) and the colorimetric test is not sensitive to phosphatidylglycerol (PG) lipids. The third fraction contained the majority of lipids, which agrees with the DCR profile. This fraction held 88 ± 2% of the initial DPPC concentration in the fluidosome formulation (19 mg/mL), with a limited lipid loss of 12 ± 2%, as assessed by the Stewart assay (see Supporting Information, Equation S1 and Equation S2).

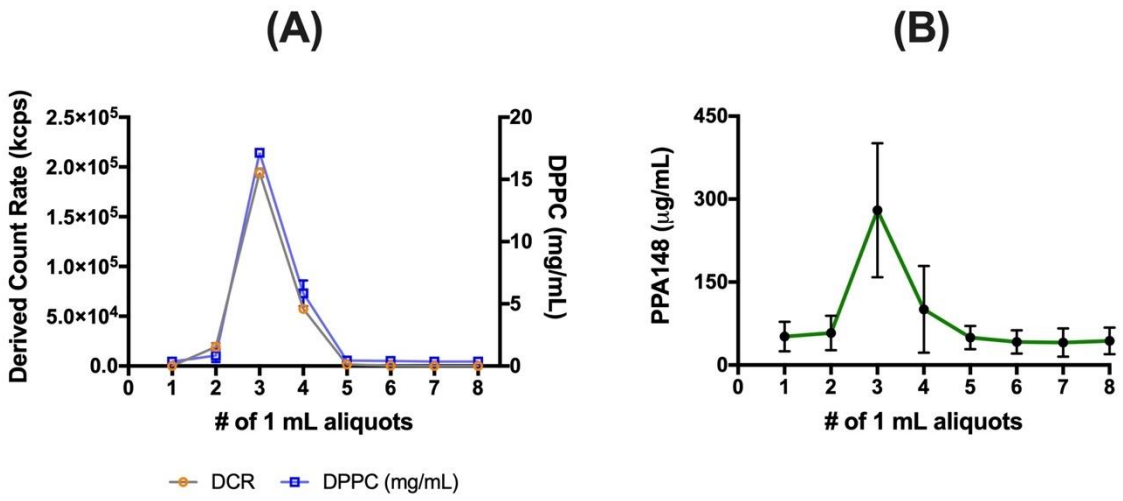

Figure 4. (A) Elution pattern of PPA148/RAMEB encapsulated fluidosomes (2.5 mg/mL) in HEPES buffered saline (pH=7.2) from the size exclusion column. The derived count rate (DCR) profile and DPPC content of fluidosomes in each aliquot were measured to investigate the elution profile of loaded liposomes. (B) Drug quantification profile of the eluted fraction from the PD10 G25 size exclusion chromatography column is presented as a function of the area under the curve (AUC). The linear calibration curve is presented in Supporting Information, Figure S5.

The third fraction contained liposomes and held 77 ± 22% of the initial lipid concentration (20 mg/mL), with a limited lipid loss of 13 ± 9%, as assessed by the Stewart assay (Equation S1 and Equation S2). The sum of lipids in all aliquots presented no overall lipid loss due to the extrusion process. The third fraction contained the highest drug content (280 ± 120 µg/mL) (Figure 4B) with encapsulation efficiency (EE) of 67 ± 11% and drug loading (DL) of 5 ± 1%. The EE and DL values of the DPPC/DMPG liposomes employed in this study were consistent with those previously reported using different drugs but similar preparation methods (51,52). The total drug concentration (590 ± 113 µg/mL) obtained from the total eluted volume from the Sephadex column is in agreement – within experimental error - with the initial drug concentration (500 µg/mL) which

was used to hydrate the lipid film. Both empty and RAMEB-encapsulating fluidosomes presented good size stability over the 10 weeks (see Supporting Information, Figure S6).

4.5 Kirby Bauer assay to assess the efficacy of PPA148-in-RAMEB-in-fluidosomes

The in vitro efficacy of the encapsulated drug/RAMEB complex in liposomes against Gram-negative bacteria was tested by using the Kirby Bauer assay. Commercially available disks of rifampicin (30 μg) and vancomycin (30 μg) were used as positive and negative controls against *E. coli* DH5a, which does not possess any antibiotic resistance genes. The in-house rifampicin disk (30 μg) caused inhibition of bacterial growth, in the same way as the commercially available disks, and was used as a positive control, while vancomycin did not affect the growth. Rifampicin is known to target the DNA-dependent RNA polymerase and passively diffuse through the cell envelope (53), and presents similar physicochemical properties with PPA148 (see Supporting Information, Table S1). Vancomycin is known to be effective against Gram-positive bacteria, but its activity against Gram-negative bacteria is hindered by its large size and the impermeable bacterial OM (54). Disks impregnated with PPA148 (1 μg/mL), rifampicin (1 and 30 μg/mL), RAMEB, PPA148/RAMEB complex, empty fluidosomes, and encapsulated fluidosomes with PPA148/RAMEB were prepared in-house. In-house rifampicin disks (30 μg/mL) were compared with the commercially available disks of the same concentration to validate the preparation method and there was no statistically significant difference (P=0.06). Figure 5 shows the inhibition zone caused by the different antimicrobials and delivery systems studied.

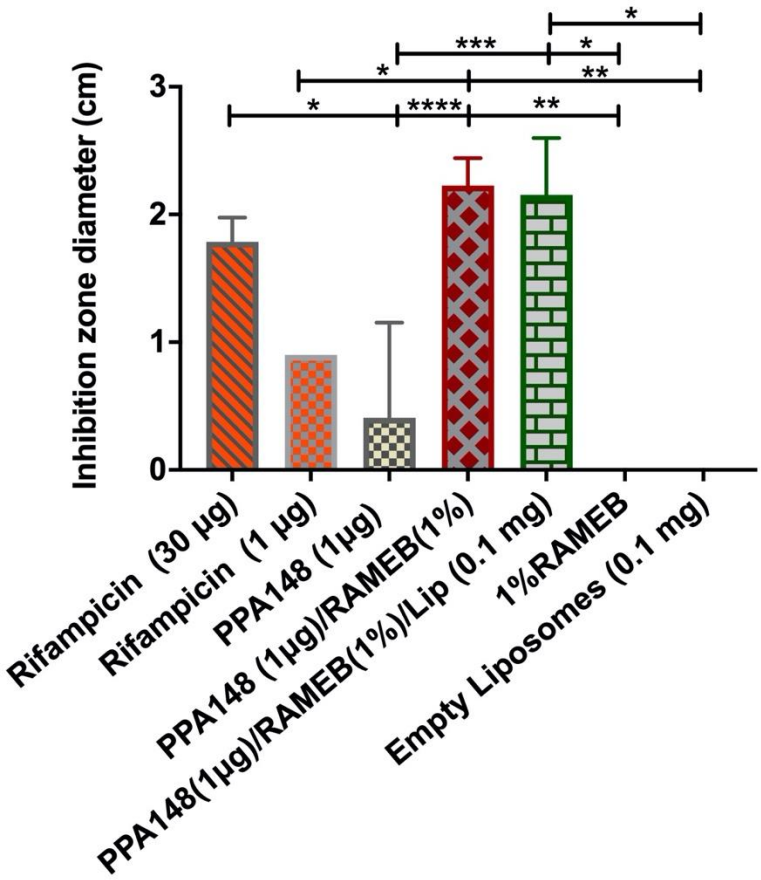

Figure 5. Kirby-Bauer assay for measuring the growth inhibition of *Escherichia coli* DH5α. The inhibition zone diameter was measured for pure rifampicin (30 µg and 1 µg) and PPA148 (1 µg) as a pure substance and as a formulated drug (in a 1% RAMEB complex and incorporated into 0.1 mg fluidosomes as a complex with 1% RAMEB) after 24 hour incubation at 37°C. Rifampicin and vancomycin were used as positive and negative control samples. The asterisks denote the level of significance going from lower to higher as follows: 0.1244 (ns), 0.0332 (*), 0.0021 (**), 0.0002 (***), <0.0001 (****). All samples were tested 12 times.

A one-way ANOVA test showed that, overall, the groups were significantly different ($p<0.0001$) at 95% confidence interval. The multiple comparison showed a clear picture within each group. Empty liposomes and pure cyclodextrin presented zero inhibition zone. There was a statistically

significant difference between the free drug, RAMEB/PPA148 complex ($p<0.0001$) and PPA148-in-RAMEB-in-liposomes ($p=0.0002$). The encapsulation of the complex into liposomes did not hinder the efficacy of the complex. Indeed, the difference between the means of the drug/CD complex alone and those encapsulated within liposomes was not statistically significant ($p>0.999$). Both the complex alone and encapsulated into liposomal vesicles presented better inhibition compared to the positive control.

4.6 Mechanistic study of the partition of the individual formulation components into the model bacterial IM and OM

4.6.1 Interaction with model OM using Gibbs isotherms

The first step in exploring the mechanism of the formulation was to examine the interaction between pure PPA148 or the carrier (fluidosomes) and model bacterial OM, as this is the first and most important permeability barrier encountered. R595 Lipid A and Rc LPS J5 monolayers were used to investigate the effect of the steric barrier of the OM outer leaflet on PPA148, rifampicin and empty fluidosomes. R595 Lipid A constitutes the membrane anchor of LPS and lacks the extended polysaccharide chain of the headgroup. After subphase injection of rifampicin to a final concentration in the trough of 20 μg/mL, the surface pressure remained constant, reflecting the lack of impact on the packing of Lipid A monolayer (Figure 6). PPA148 produced an increase in surface pressure of 6.9 ± 0.7 mN/m, reaching a plateau in less than an hour with a high binding affinity (Hill slope = 1.3 ± 0.2), thus denoting some interaction between the drug and the monolayer (Figure 6). In the presence of Rc LPS J5 monolayers, the increase in surface pressure is weaker, showing low efficiency ($\Delta\Pi_{max}$ = 3.7 ± 2.1 mN/m), weak binding capacity (Hill slope = 3.7 ± 2.6) but a fast rate of binding with $t_{50\%}$ = 0.2 ± 0.1 h (Figure 6). Being a lipophilic drug,

PPA148, was expected to adsorb on the air/liquid interface between the lipids as it did on a lipid free interface (see Supporting Information, Figure S7), which produced an increase in surface pressure of 13.3 ± 1.3 mN/m with $t_{50\%}$ = 0.3 ± 0.2 h.

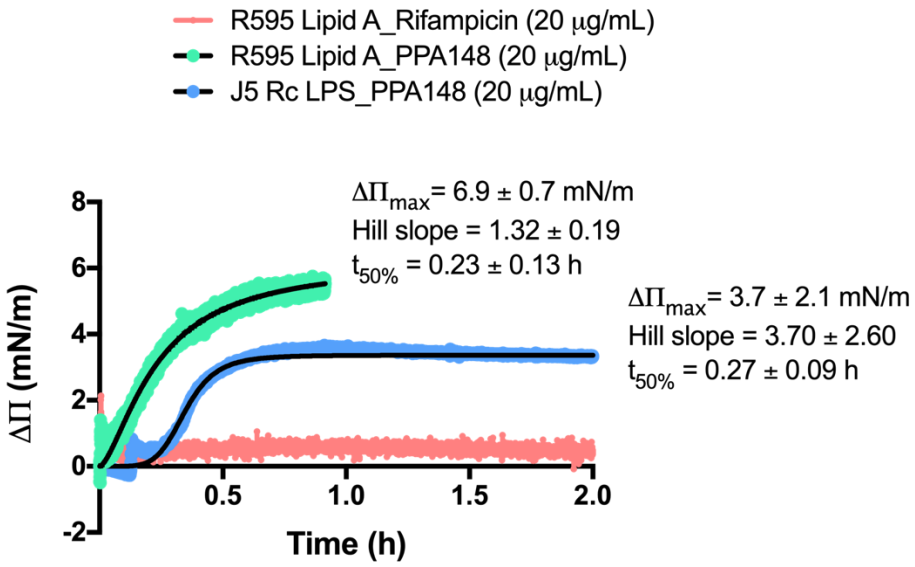

Figure 6. Representative Gibbs isotherms at 23 ± 1 °C of PPA148 and rifampicin using R595 Lipid A extracted from *Salmonella minnesota* and Rc J5 LPS extracted from *E. coli* monolayers and 1 mM $MgCl_2$ as a subphase. Both Lipid A and LPS monolayers were compressed at a surface pressure of 30-35 mN/m and the drugs were used at a concentration of 20 μg/mL and the black lines are the fitted curves based on the mathematical model.

The carrier of the drug/CD complex, fluidosomes, were tested on model bacterial OM to investigate their mechanism of action. Preliminary results revealed the adsorption of fluidosomes on lipid free surface (HEPES buffered saline containing $CaCl_2$) and the R595 Lipid A monolayer. In the absence of lipid monolayer, fluidosomes adsorbed on the clean surface, reaching a change in surface pressure of 11.0 ± 4.8 mN/m. An increase in surface pressure was also observed after injecting fluidosomes below the R595 Lipid A monolayer ($\Delta\Pi_{max}$ = 6.3 ± 1.9 mN/m). The speed

and affinity towards both lipid free surface and R595 Lipid A monolayers are high and of the same magnitude (hill slope of 1.0 ± 0.4 and 0.4 ± 0.3 respectively) (Figure 7). However, fluidosomes caused solubilization of Rc J5 LPS monolayer. The surface pressure dropped to -10.4 ± 1.3 mN/m within 3 h, which illustrates removal of the lipids from the surface. Precipitation of lipids in the subphase was observed visually in the petri dish.

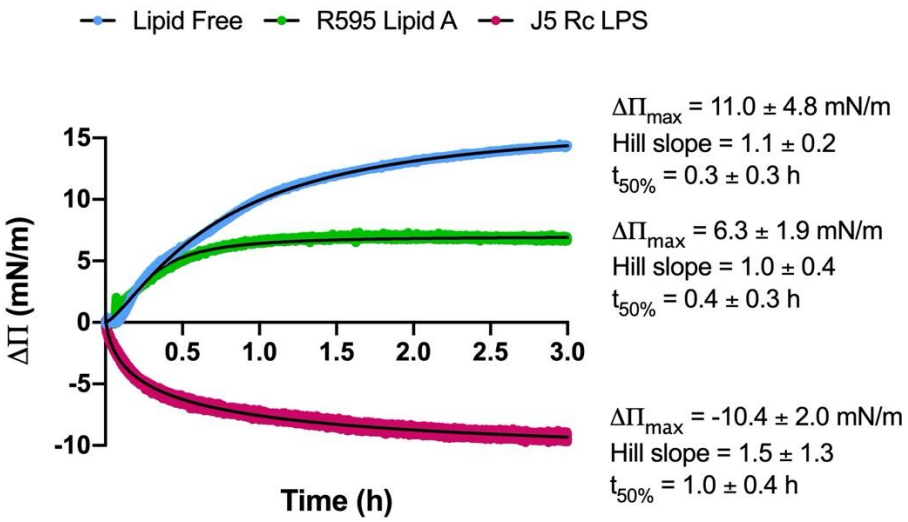

Figure 7. Representative adsorption and Gibbs isotherms at 23 ± 1 °C of 0.1 mg/mL fluidosomes using 20 mM HEPES buffered saline containing 2 mM $CaCl_2$ as a subphase (lipid free solution) and two different lipid monolayers to mimic the outer leaflet of the OM: Rc J5 LPS extracted from *E. coli* and R 595 Lipid A extracted from *Salmonella minnesota*. Both Lipid A and LPS monolayers were compressed at a surface pressure of 30-35 mN/m. The black line in lipid free and R595 Lipid A curves is the fitted curve based on the mathematical model.

To support the choice of liposomes as carriers, RAMEB and HPβCD were tested against LPS and Lipid A monolayers (see Supporting Information, Figure S8). The results revealed that the solubilizing effect of fluidosomes is stronger than that of cyclodextrins. Particularly, R595 Lipid

A or J5 Rc LPS monolayers remained undisturbed by HPβCD, while RAMEB induced a weak interaction, inducing a decrease in surface pressure to ~ -5 mN/m.

4.6.2 Interaction with model IM using Gibbs isotherms

Cyclodextrins are expected to enhance the permeation of PPA148 through the IM of the bacterial membrane (16). Gibb's isotherms were used to examine the molecular interaction of unformulated PPA148 (20 μg/mL) and the pure β-cyclodextrin derivatives, RAMEB and HPβCB, with model IM, namely, DPPC/DPPG, in order to mimic the composition of the leaflets of the inner membrane of the bacterial cell envelope. Rifampicin was used as a model drug to compare with the novel antibiotic.

DPPC/DPPG mixtures were spread on a small trough surface to form a monolayer. The starting surface presure created by the lipid spread was 30-35 mN/m to be equivalent to the lateral pressure of the bacterial inner membrane (42). An increase in surface pressure of the monolayer was observed, after introducing either of the drugs into the subphase (Figure 8A). PPA148 produced a smaller change in surface presure of ~3.7 mN/m, compared to ~15.8 mN/m for rifampicin. A different kinetic profile was observed by comparing the Hill slopes of each drug's Gibbs isotherm, i.e. 3.7 ± 2.6 for PPA148 and 0.85 ± 0.25 for rifampicin. PPA148 interacted faster than rifampicin, which was not expected, given the similar physicochemical properties of the two drugs (see Supporting Information, Table S1).

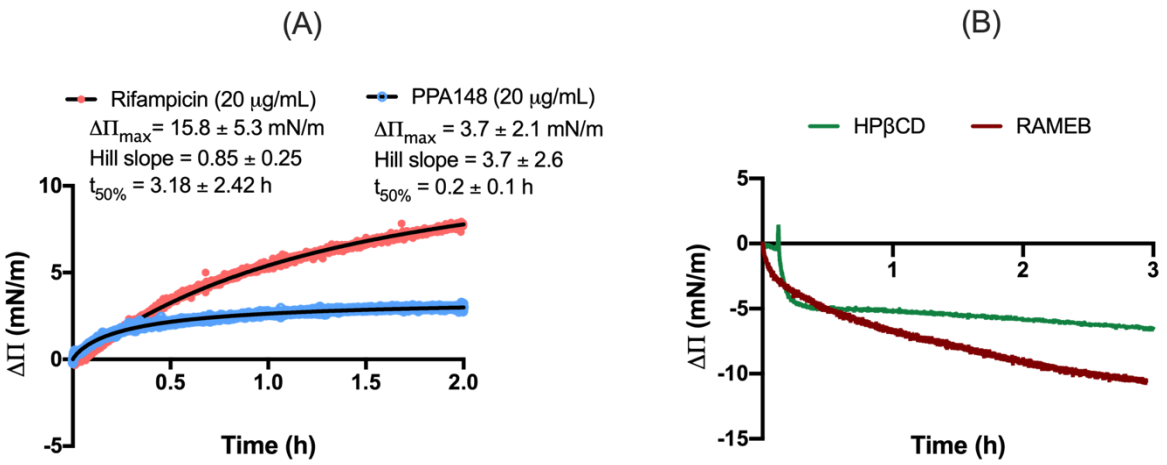

Figure 8. Representative Gibbs isotherms at 23 ± 1 °C of (A) PPA148 and rifampicin and (B) RAMEB and HPβCD using DPPC/DPPG (3:1) monolayer and 1 mM $MgCl_2$ as a subphase. The drugs were used at a concentration of 20 μg/mL and the cyclodextrin were tested at 1% w/v. The black lines in (A) are the fitted curves based on the mathematical model.

HPβCD and RAMEB showed a solubilization effect on all lipid monolayers by eliciting a negative change in their initial surface pressure. DPPC/DPPG (3:1) monolayers underwent a significant loss of molecules from the surface when challenged with HPβCD and RAMEB (Figure 8B).

4.7 Interaction with model OM using neutron reflectivity

NR was used to further explore the effect of fluidosomes on a model asymmetric bilayer representing the Gram-negative OM (Figure 9, Table 2) (44,49,55). The structure of the model membrane was characterized at 38°C prior to and after being challenged with the liposomal carrier (hydrogenated DPPC/DMPG at a molar ratio of 18:1). The interface was modelled as a series of slabs each representing a different layer of the model OM with individual SLD, thickness, hydration and roughness (Figure 9A, C). The best-fit of each parameter was obtained from the

Bayesian analysis with 95% confidence intervals which is presented in SI (see Supporting Information, Table S2, Figure S10).

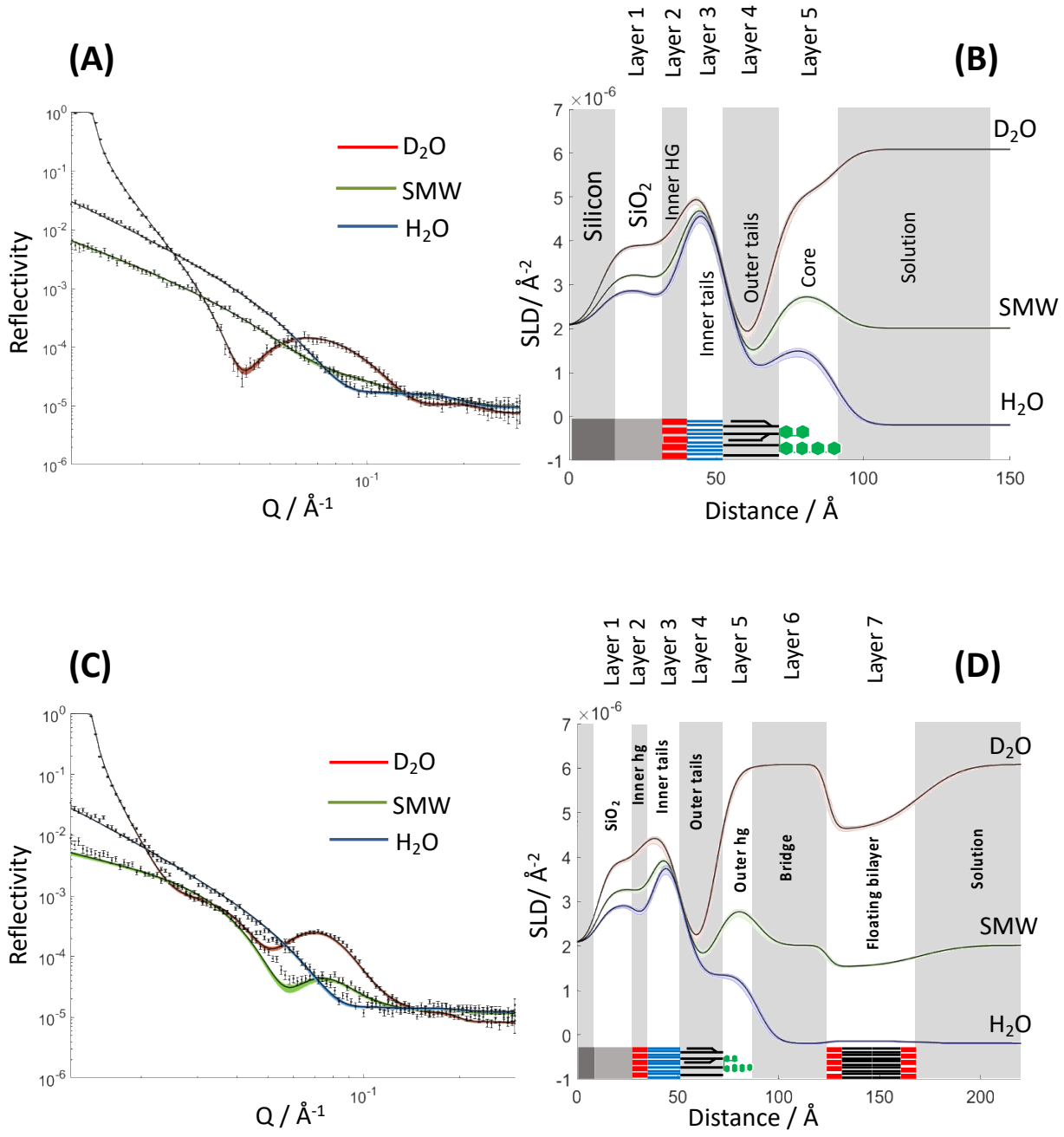

Figure 9. Neutron reflectivity profile (A, C) and model data fits with their scattering length density profiles (B, D) for an asymmetrically deposited d_{62}DPPC (inner leaflet) and hydrogenous Ra-LPS

(outer leaflet) model membrane before (A, B) and after (C, D) being challenged with 0.1 mg/mL hydrogenous fluidosomes (DPPC/DMPG, 18:1) at 38 °C. The sample was measured in three isotopic contrasts (D_2O, H_2O and SMW). The model membrane was fitted into a seven-layered mathematical model: Silicon oxide (SiO_2), DPPC headgroup (Inner HG), DPPC tails (Inner tails), Ra LPS tails (Outer tails) and Ra LPS headgroups (Core), Bridge and Floating bilayer.

Figure 9A shows the reflectivity and SLD profile of the model outer membrane at 38°C. The NR data were fitted to a five-layer model, thereby using the minimal number of layers with which the reflectivity data could be fitted. The interference fringe observed in the D_2O contrast (Figure 9A) indicates the presence of the bilayer. The layers, presented schematically under the fitted SLD curves in Figure 9B, are the silicon, silicon oxide, inner d_{62}DPPC headgroups which are hydrogenated, inner d_{62}DPPC tails, outer Ra-LPS tails, outer Ra-LPS headgroup (headgroup) and bulk solution. The results reveal that a highly asymmetric lipid bilayer was formed on the silicon oxide-coated surface of the substrate.

The fusion mechanism of the fluidosomes with the bacterial membrane was investigated by measuring changes in the structure of the fully characterized d_{62}DPPC:h-Ra-LPS bilayer after being challenged with 0.1 mg/mL empty fluidosomes for 1 h. Most of the structural changes occurring following the addition of fluidosomes involved the tail and outer headgroup regions of the lipids. The exposure of the bilayer to fluidosomes resulted in the addition of a fringe in the reflectivity profile (Figure 9C), reflecting the presence of two lipid bilayers (Figure 9D), one being the OM model and the second being described as a floating bilayer (6th and 7th layer), which is a result of liposomes being attached on the outer Ra-LPS headgroups, in the SLD profile.

Table 2. Best-fit values of structural parameters (obtained from the Bayesian analysis with 95% confidence interval) of the challenged Ra-LPS/DPPC membrane at 38°C derived from fits to the neutron reflectivity data shown in Figure 9. The min and max values of each parameter are presented in Supporting Information, Table S2.

Layer	Asymmetric bilayer at 38 °C					
	Before challenge			After challenge		
	Thickness (Å)	% water	Roughness (Å)	Thickness (Å)	% water	Roughness (Å)
SiO2	20.1	16.3	4.6	20.1	16.3	4.6
Inner HG	7.4	28.3	6.4	5.8	48.4	7.2
Inner Tails	14.7	1.3		15.3	0.03	
Outer Tails	14.8			16.8		
Outer HG/Core	23.1	51.8		21.1	36.0	

Bridge	n/a	n/a	n/a	34.6	99.9	3.4
Vesicles/Bilayer	n/a	n/a	n/a	45.8	75.8	16.6

Of the two additional layers formed, the one adjacent to the membrane is a solvent layer (99.94% water content) as reflected by its SLD being close to zero, i.e. 0.18×10^{-6} Å^{-2}, indicating that it is composed of mostly hydrogenous material. This solvent layer is described by a thickness of 34.6 Å and roughness of 3.4 Å. The outermost layer has high water content (75.80%) with an SLD of 0.03×10-6 Å^{-2}. If the liposomes were intact on the membrane surface, their tail SLD would have been similar to the reported SLD of h-DPPC tails (-0.4×10^{-6} Å^{-2}) as published by Clifton and coworkers (44). The thickness of the additional layers was found to be 35 and 46 Å for the 6th and 7th layer, respectively. The 7th layer presented a curved bilayer because its thickness (46 Å) is 2 Å less than that of a DPPC bilayer (approximately 50-60 Å) in the presence of $CaCl_2$ (41,56,57) . The possible structural changes in the model asymmetric OM may infer to a bridge layer and are schematically represented in Figure 10.

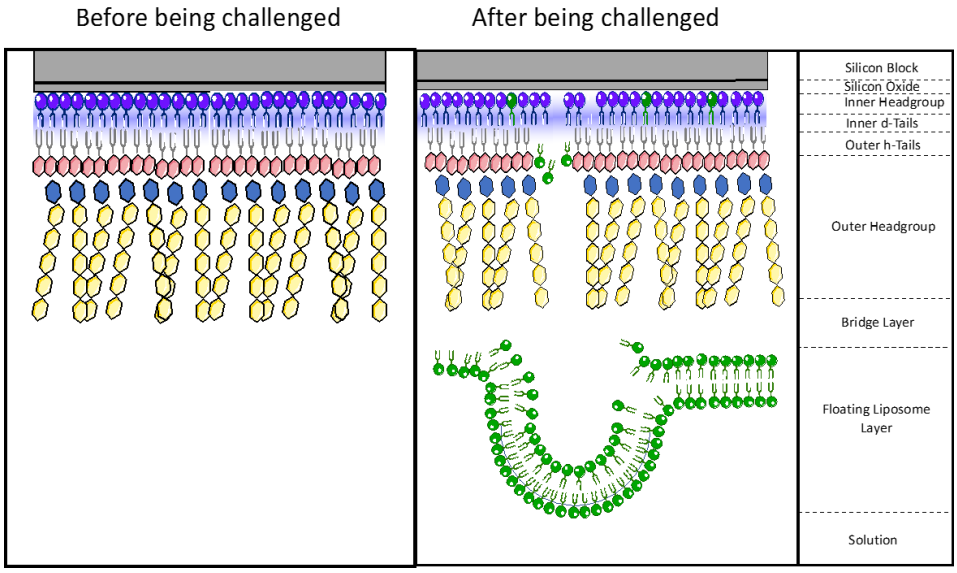

Figure 10. Representation of the possible structural changes in the model OM system after being challenged by fluidosomes.

The volume fraction of water and lipids within the bilayer region show that mixing of the lipids occurred as reflected by the lipid composition in the model membrane (Table 3). The contribution of hydrogenous phospholipids in the inner leaflet layers, which may be either h-Ra LPS or h-phospholipids from fluidosomes, increased from 21% before challenge to 35% after adding the fluidosomes (Table 3). The hydration of the bilayer decreased from 1.26% to 0.03% and of the outer headgroup decreased from 51.77% to 35.97% (Table 2 and Table 3).

Table 3. Volume fraction of deuterated DPPC tails ($\boldsymbol{\varphi_{DPPC}}$), hydrogenous LPS tails ($\boldsymbol{\varphi_{RaLPS}}$) and water ($\boldsymbol{\varphi_{water}}$) within the bilayers of Ra-LPS/d-DPPC 38°C before and after the challenge by the fluidosomes. Each parameter was obtained with 95% confidence interval which are presented in the SI. The min and max values of each parameter are presented in Supporting Information, Table S2.

<table>
<tr><th rowspan="3">Layer</th><th colspan="6">Asymmetric bilayer at 38 °C</th></tr>
<tr><th colspan="3">Before challenge</th><th colspan="3">After challenge</th></tr>
<tr><th>$\boldsymbol{\varphi_{DPPC}}$</th><th>$\boldsymbol{\varphi_{RaLPS}}$</th><th>$\boldsymbol{\varphi_{water}}$</th><th>$\boldsymbol{\varphi_{DPPC}}$</th><th>$\boldsymbol{\varphi_{RaLPS}}$</th><th>$\boldsymbol{\varphi_{water}}$</th></tr>
<tr><td>SiO2</td><td>n/a</td><td>n/a</td><td>0.16</td><td>n/a</td><td>n/a</td><td>0.16</td></tr>
<tr><td>Inner Headgroup
Inner Tails</td><td colspan="2">0.78 0.21</td><td rowspan="2">0.013</td><td colspan="2">0.65 0.35</td><td rowspan="2">0.0003</td></tr>
<tr><td>Outer Tails
Outer Headgroup
(Core)</td><td colspan="2">0.14 0.85</td><td colspan="2">0.21 0.79</td></tr>
</table>

5 DISCUSSION

Solubility is a major challenge in drug development and pre-formulation science. PPA148 is a newly synthesized C8-substituted PBD derivative which presents promising activity against Gram-negative bacteria. The broader PBD family is known for its poor aqueous solubility due to the high number of aromatic rings in their structure, (24) making them soluble in either organic solvents, such as chloroform and DCM, or in aqueous solutions containing water-miscible organic solvents, such as DMSO and acetonitrile (58). PPA148 is no exception, and possesses a low water solubility (30 μg/mL) necessitating the use of DMSO as a solvent in biological assays (MIC and time-kill curves) (12). This led us to investigate the use of delivery systems to try to improve PPA148 solubility and thus bioavailability and efficacy.

When considering suitable vehicles for the delivery of antimicrobials, liposomes represent an attractive option, having been successfully used as carriers for antifungal (AmBisome®, Abelet® and Amphotec®) and antibiotic (TOVI® Podhaler and Bethkis®) delivery to enhance efficiency and stability (59). Cyclodextrins, on the other hand, although widely used for drug solubilization through inclusion complex formation, in particular with the antifungal itraconazole (Sporanox®), are not currently used in commercial antibiotic products. Nevertheless, some studies on the antimicrobial activity of cyclodextrins have reported both an improvement of drug solubility (60) and permeability into cell membranes (16). The combination of both components, liposomes and cyclodextrins, offers a superior formulation which, to our knowledge, has not yet been investigated on antibiotic delivery. This research suggests that ACL offers improved stability of liposomes in the presence of cyclodextrins, suppresses the concentration and competitive effect on the dissociation of drug/CD complex and finally provides specificity to bacterial cells through Ca^{2+} bridges between the fluidosomes and the bacterial envelope.

In this study, β-cyclodextrin derivatives, HPβCD and RAMEB, were successfully used to improve the solubility of PPA148, up to approximately 50 μg/mL and 90 μg/mL, respectively, forming a 1:2 complex. PPA148 presented a higher affinity towards RAMEB compared to HPβCD, which is attributed to the hydrophobic microenvironment provided by the methyl substitution (61); this derivative was thus taken forward for combination with liposomes. The RAMEB/PPA148 complex was incorporated into fluid liposomes (DPPC/DMPG of 18/1) with an encapsulation efficiency of 67 ± 11% and drug loading of 5 ± 1%.

The *in vitro* Kirby Bauer assay revealed an increased efficacy of the novel antibiotic formulated in cyclodextrins compared to non-formulated drug against *E. coli* DH5α. RAMEB alone did not lead to bacterial growth inhibition, showing that it may work as a permeability enhancer to increase drug update by Gram-negative bacteria. Previous work has also reported increased drug potency against Gram-negative bacteria by using inclusion complexes of β-lactam antibiotics with different types of cyclodextrins (62). While the mechanism of action of cyclodextrins has not yet been clarified, it has been reported that β-CD may drive the internalization of the β-CD-antibiotic complex via (i) enhanced adhesion to the bacterial surface with local release of the antibiotic, and (ii) destabilization of the bacterial envelope (62–64). The former behavior was evidenced in this study by examining the interfacial adsorption of RAMEB on model IM monolayers. The efficacy of PPA148-in-RAMEB-in-fluidosome was not statistically different from that of the PPA148/RAMEB complex. Nevertheless, fluidosomes offer specificity to the Gram negative bacterial membrane, as shown by the interfacial studies, and may protect the complex from dissolution and dissociation (65), thus preventing a possible reduction in bioavailability during delivery. In addition, the entrapment of the water-soluble inclusion complex into fluidosomes led to the accommodation of the insoluble PPA148 in the aqueous phase of the vesicles. It is worth

noting that PPA148-in-RAMEB-in-fluidosome (1 μg PPA148), showed equivalent efficacy to pure rifampicin (30 μg).

The interactions between PPA148, cyclodextrins and fluidosomes with model bacterial membranes were measured using interfacial techniques. The Gram-negative bacterial envelope consists in part of two permeability barriers, the first being the LPS-containing asymmetric OM, and the second being phospholipid-containing IM, separated by the peptidoglycan-containing periplasm. In the monolayer studies, Rc J5 LPS extracted from *E. coli* and Lipid A extracted from the Re R595 *S. minnesota* were used to mimic the outer leaflet of the OM and to examine the steric hindrance created by the presence of the core oligosaccharide chain in the former. A mixture of DPPC/DPPG was used to mimic the IM. Fluidosomes were tested against model OM as it is the carrier of the drug/CD complex and is proposed to release its payload in the cytoplasmic space, while cyclodextrin was tested against model IM as it is incorporated in the liposomes and is suggested to enhance the transport of PPA148 through the cytoplasmic barrier (IM). PPA148 was tested against both the outer and inner model membranes.

The Gibbs isotherms provided useful insights into the molecular interactions of the drug, RAMEB and HPβCD on phospholipid monolayers, either at the level of the polar region when they are in contact with the IM of the cell envelope, or at the level of the hydrophobic domain of the lipid bilayer. Although PPA148 adsorbs strongly at the bare interface, its adsorption at the lipid/air interface is weaker, which reflects the effect of steric hindrance from the lipids. Between the two lipid monolayers tested, the interaction of PPA148 with model IM shows a higher affinity towards the DPPC/DPPG monolayer than the model outer leaflet of the OM. This could be attributed to the smaller headgroup of DPPC/DPPG, leading to a weak steric hindrance to PPA148 and a stronger interaction. PPA148 showed a weak interaction with Rc J5 LPS and R595 Lipid A.

Interestingly, the adsorption of PPA148 in the R595 Lipid A, which lacks the core oligosaccharide, caused a larger change in surface pressure than with Rc J5 LPS. This suggests that the core polysaccharide region of the Rc J5 LPS creates a steric barrier, hindering the interfacial adsorption of PPA148. The high affinity of PPA148 with lipid A reflects the effect of steric hindrance on drug's interaction with model lipid membranes and confirms the need of a formulation to overcome the limited permeation of both barriers.

PPA148 and rifampicin present a different interaction profile with both model OM and IM monolayers. The findings for rifampicin, that it was attracted to the phospholipid monolayer (DPPC/DPPG [3/1]) partially but did not interact with model OM, are in agreement with its mechanism of transport: it does not partition in the OM but it partitions in DPPC monolayers via electrostatic attraction with the headgroups of DPPC in an acidic environment (pH=5) (66). PPA148 cannot be ionized and thus the Gibbs isotherm in model IM reveals a weaker but faster interaction compared to rifampicin, possibly due to the absence of ionic bonds. It is suggested that PPA148 is likely to enter the cell via diffusion through the membrane due to its high hydrophobicity. However, its diffusion is hindered by the steric effect of LPS.

The interaction of HPβCD and RAMEB with phospholipid monolayers suggest a lipid-solubilizing effect of model IM monolayers, whereas little effect was found for the model OM monolayers. It was found that upon cyclodextrin-membrane interaction, the type of βCD derivative affects the efficiency of the interaction with DPPC/DPPG monolayer, with HPβCD showing a weaker interaction. RAMEB shows a high affinity towards the DPPC/DPPG monolayer, which was expected because RAMEB has been reported to induce phospholipid exchange more efficiently than HPβCD (67). In addition, it has also been reported that RAMEB forms soluble complexes with DPPC (68), which explains the negative surface pressure of the isotherm. It is proposed that

RAMEB interacts with the phospholipids of the IM without causing any defects on the membrane while releasing PPA148 in the cytoplasm, in which the intracellular target is located.

The fluidosomes presented different interaction profiles in the presence and absence of steric hindrance. The air/liquid interface monolayer interaction experiment revealed adsorption of material on a lipid free surface and the R595 Lipid A monolayer, while lipid solubilization took place with the Rc J5 LPS monolayer. It has been reported that the aggregation and fusion of fluidosomes with Gram-negative bacterial membrane is promoted by the presence of Ca^{2+} or other divalent cations by inducing the neutralization of the negatively charged Lipid A and dehydration of phospholipids of the membrane (22). It has been found that LPS becomes exposed to fluidosomes in the presence of divalent cations by changing the orientation of its oligosaccharide chains, which become parallel with the interface (22). These results suggest that fluidosomes composed of DPPC/DMPG [18/1] could release their content by fusion into the OM membrane, as also found with a DPPC/DMPG [9/1] system by negative staining and lipid mixing assay with fluorescence probes (22). This bridging by Ca^{2+} ions between the bacterial envelope and fluidosomes may also constitute a means of ensuring specificity of the delivery system to bacterial cells.

To complement these monolayer studies and further investigate the putative fluidosome fusion mechanism, a model Gram-negative bacterial asymmetric membrane consisting of Ra LPS and DPPC as the outer and inner leaflet of the OM was used to examine the interaction between the liposomal carrier and the OM (44,47,49). Neutron reflectivity (NR) was used to characterize the structural changes in this model membrane when placed in contact with the formulation. The challenge of the model OM by fluidosomes caused an increase of hydrogenous material in the

inner leaflet and an increase of deuterated material in the outer leaflet, which reveal the occurrence of lipid mixing within the membrane.

Moreover, the formation of an additional curved bilayer associated with the deposited membrane was observed after a challenge by the fluidosomes. It has been reported that cations (Ca^{2+}, Mg^{2+}) trigger the fusion of liposomes in bacterial membranes through bridging of the layers between the outer leaflets of the membrane and liposome at the contact site (Figure 10) (22). It has been reported that Ca^{2+} are able to keep fluidosomes attached to the model membrane by creating local packing defects on the outer leaflet of both liposomes and LPS (Figure 10) accompanied by local dehydration (22), as observed by a decrease in the percentage of water of the Ra LPS headgroup. This strengthens evidence obtained from the monolayer studies for a possible mechanism of fluidosomes specificity to the bacterial envelope. Moreover, fluidosomes composed of DPPC/DMPG [18/1] tend to become more fluid around 38°C (Tm of 35°C) which also aids their fusion with the bacterial OM (23) (22).

The findings reveal that ACL shows the potential to target both the outer and the inner membrane by combining two delivery systems in one carrier. Theoretically, fusion of fluidosomes with the OM facilitate the release of its core content (RAMEB/PPA148 complex) into the periplasm. RAMEB, in addition to increasing drug's water solubility, would then be able to potentiate the transport of PPA148 to effect penetration of the antibiotic through the IM (phospholipid bilayer), without causing any damage to the membrane and thus allowing PPA148 to reach its intracellular target. NR showed that fusion of fluidosomes is created by a bridge layer between the outer leaflets of the membrane (LPS) and liposomes (DPPC/DMPG [18/1]) in the presence of Ca^{2+}, while microbiological and interaction studies showed that RAMEB improves the adhesion to bacterial surface and drug's transport through phospholipid layers without causing any damage to the

membrane. From a biophysical point of view, each compartment of the formulation was tested separately to investigate the putative mechanism of action. However, there is a need for future investigation on drug/RAMEB complex and ACL interaction with model bacterial membranes to achieve a complete picture of the proposed mechanism.

6 CONCLUSION

This work is the first report of an antibiotic-in-cyclodextrin-in-liposome (ACL) formulation using the novel hydrophobic antimicrobial agent PPA148, which shows promising activity against Gram-negative bacteria. The water solubility of the drug was enhanced by interaction with two modified β-cyclodextrins, HPβCD and RAMEB. Although ACL did not present significant difference in inhibition of bacteria compared to the drug/CD complex itself, it interacts with both the OM and IM of bacterial envelope and its proposed mechanism of action was examined at the molecular level, using interfacial techniques. Our results suggest that fluidosomes act as carriers of the complex, fusing into the OM and thus facilitating the release of their payload, while RAMEB also enables transport through the IM. Neutron reflectivity were successfully used to demonstrate the possible envelope-breaching mechanism of fluidosomes upon interaction with the model OM.

The molecular understanding of ACL provided in this work demonstrate their promise as hydrophobic antimicrobial agents, either new drugs, or those that have become ineffective due to antimicrobial resistance. ACL formulations may contribute to the fight against AMR because they target both the OM and IM of Gram-negative bacteria, while enhancing the solubility of drugs and thus increasing their bioavailability.

ASSOCIATED CONTENT

Supporting Information

Table of physicochemical properties of PPA148 and best fit parameter values with 95% confidence interval for the NR fits.

Figures of absorbance of increasing PPA148 concentration, effect of increasing concentration of PPA148 on particle size when the drug is in H2O and HPβCD, ^{1}H NMR spectra used to plot Job's plot, intensity distribution of empty DPPC/DMPG (18/1) liposomes in HEPES buffered saline (pH 7.2), linear calibration curve of the area under the curve (AUC) of PPA148, fluidosome stability, adsorption of PPA148 at the air/liquid interface, Gibs isotherms of cyclodextrins and model OM monolayers, Langmuir trough isotherm cycles for the NR preparation of model membranes and posterior distributions for all the layers of the NR systems.

Equations used in the quantification of Stewart assay to quantify and calculate the DPPC concentration.

ACKNOWLEDGMENT

The NR work was supported by neutron beam time at ISIS STFC, Didcot, UK., (experiment reference number: 1710319, DOI: 10.5286/ISIS.E.RB1710319).

REFERENCES

1. Levy SB, Marshall B. Antibacterial resistance worldwide: causes, challenges and responses. Nat Med. 2004 Dec;10(12s):S122–S129.

2. Piddock LJV. Clinically Relevant Chromosomally Encoded Multidrug Resistance Efflux Pumps in Bacteria. Clin Microbiol Rev. 2006 Apr;19(2):382–402.

3. Fernandez L, Hancock REW. Adaptive and Mutational Resistance: Role of Porins and Efflux Pumps in Drug Resistance. Clin Microbiol Rev. 2012 Oct;25(4):661–681.

4. Bolla J-M, Alibert-Franco S, Handzlik J, Chevalier J, Mahamoud A, Boyer G, et al. Strategies for bypassing the membrane barrier in multidrug resistant Gram-negative bacteria. FEBS Lett. 2011 Jun;585(11):1682–1690.

5. WHO publishes list of bacteria for which new antibiotics are urgently needed [Internet]. [cited 2018 Oct 6]. Available from: http://www.who.int/news-room/detail/27-02-2017-who-publishes-list-of-bacteria-for-which-new-antibiotics-are-urgently-needed

6. Spellberg B, Shlaes D. Prioritized Current Unmet Needs for Antibacterial Therapies. Clin Pharmacol Ther. 2014;96(2):151–3.

7. Mantravadi PK, Kalesh KA, Dobson RCJ, Hudson AO, Parthasarathy A. The Quest for Novel Antimicrobial Compounds: Emerging Trends in Research, Development, and Technologies. Antibiotics. 2019 Mar;8(1):8.

8. Baptista PV, McCusker MP, Carvalho A, Ferreira DA, Mohan NM, Martins M, et al. Nano-Strategies to Fight Multidrug Resistant Bacteria—"A Battle of the Titans." Front Microbiol [Internet]. 2018 Jul 2 [cited 2019 Nov 11];9. Available from: https://www.ncbi.nlm.nih.gov/pmc/articles/PMC6036605/

9. Andriollo P, Hind CK, Picconi P, Nahar KS, Jamshidi S, Varsha A, et al. C8-Linked Pyrrolobenzodiazepine Monomers with Inverted Building Blocks Show Selective Activity against Multidrug Resistant Gram-Positive Bacteria. ACS Infect Dis. 2018 Feb 9;4(2):158–74.

10. Rahman KM, Rosado H, Moreira JB, Feuerbaum E-A, Fox KR, Stecher E, et al. Antistaphylococcal activity of DNA-interactive pyrrolobenzodiazepine (PBD) dimers and PBD-biaryl conjugates. J Antimicrob Chemother. 2012 Jul;67(7):1683–96.

11. Picconi P, Jeeves R, Moon CW, Jamshidi S, Nahar KS, Laws M, et al. Noncytotoxic Pyrrolobenzodiazepine–Ciprofloxacin Conjugate with Activity against Mycobacterium tuberculosis. ACS Omega. 2019 Dec 3;4(25):20873–81.

12. Rahman KM, Sutton JM, Picconi P. Pbd antibacterial agents. WO 2017/098257 Al, 2017.

13. Jambhekar SS, Breen P. Cyclodextrins in pharmaceutical formulations II: solubilization, binding constant, and complexation efficiency. Drug Discov Today. 2016 Feb 1;21(2):363–8.

14. Agnes M, Thanassoulas A, Stavropoulos P, Nounesis G, Miliotis G, Miriagou V, et al. Designed positively charged cyclodextrin hosts with enhanced binding of penicillins as carriers for the delivery of antibiotics: The case of oxacillin. Int J Pharm. 2017 Oct;531(2):480–491.

15. Paczkowska M, Mizera M, Szymanowska-Powa\lowska D, Lewandowska K, B\laszczak W, Gościańska J, et al. β-Cyclodextrin complexation as an effective drug delivery system for meropenem. Eur J Pharm Biopharm. 2016 Feb;99:24–34.

16. Shastri VR, Yue I, Hildgen P, Sinistera RD, Langer R. Method of increasing the efficacy Of Antibiotics By Compexing With Cyclodextrins. US2003/0078215A1., 2003.

17. European Medicines Agency C for HMP (CHMP). Cyclodextrins used as excipients. European Medicines Agency; 2017 Oct p. 16. Report No.: EMA/CHMP/495747/2013.

18. Stella VJ, Rao VM, Zannou EA, Zia V. Mechanisms of drug release from cyclodextrin complexes. Adv Drug Deliv Rev. 1999 Mar 1;36(1):3–16.

19. Serna JB de la, Perez-Gil J, Simonsen AC, Bagatolli LA. Cholesterol Rules Direct Observation of the Coexistence of Two Fluid Phases in Native Pulmonary Surfactant Membranes at Physiological Temperatures. J Biol Chem. 2004 Sep 24;279(39):40715–22.

20. Gharib R, Greige-Gerges H, Fourmentin S, Charcosset C, Auezova L. Liposomes incorporating cyclodextrin–drug inclusion complexes: Current state of knowledge. Carbohydr Polym. 2015 Sep;129:175–186.

21. Sachetelli S, Khalil H, Chen T, Beaulac C, Sénéchal S, Lagacé J. Demonstration of a fusion mechanism between a fluid bactericidal liposomal formulation and bacterial cells. Biochim Biophys Acta. 2000 Feb;1463(2):254–66.

22. Wang Z, Ma Y, Khalil H, Wang R, Lu T, Zhao W, et al. Fusion between fluid liposomes and intact bacteria: study of driving parameters and in vitro bactericidal efficacy. Int J Nanomedicine. 2016;11:4025–4036.

23. Desjardins A, Chen T, Khalil H, Sayasith K, Lagacé J. Differential Behaviour of Fluid Liposomes Toward Mammalian Epithelial Cells and Bacteria: Restriction of Fusion to Bacteria. J Drug Target. 2002 Jan;10(1):47–54.

24. Picconi P, Rahman KM, Coates A, Sutton M. Design, Synthesis and Biological Evaluation of Minor Groove Binders as Antibacterial Agents Against Multi-Drug Resistant Pathogens. 2017.

25. Valero M, Castiglione F, Mele A, da Silva MA, Grillo I, González-Gaitano G, et al. Competitive and Synergistic Interactions between Polymer Micelles, Drugs, and Cyclodextrins: The Importance of Drug Solubilization Locus. Langmuir ACS J Surf Colloids. 2016 13;32(49):13174–86.

26. Nigam S, Durocher G. Spectral and Photophysical Studies of Inclusion Complexes of Some Neutral 3H-Indoles and Their Cations and Anions with β-Cyclodextrin. J Phys Chem. 1996 Jan;100(17):7135–7142.

27. Peeters J, Neeskens P, Tollenaere JP, Van Remoortere P, Brewster ME. Characterization of the interaction of 2-hydroxypropyl-β-cyclodextrin with itraconazole at pH 2, 4, and 7. J Pharm Sci. 2002 Jun;91(6):1414–1422.

28. Huang CY. Determination of binding stoichiometry by the continuous variation method: The job plot. Methods Enzymol. 1982 Jan;87:509–525.

29. Bertholet P, Gueders M, Dive G, Albert A, Barillaro V, Perly B, et al. The effect of cyclodextrins on the aqueous solubility of a new MMP inhibitor: phase solubility, 1 H-NMR

spectroscopy and molecular modeling studies, preparation and stability study of nebulizable solutions. J Pharm Pharm Sci Publ Can Soc Pharm Sci. 2005 Jul;8(2):163–174.

30. Hirayama F, Kurihara M, Horiuchi Y, Utsuki T, Uekama K, Yamasaki M. Preparation of heptakis(2,6-di-O-ethyl)-beta-cyclodextrin and its nuclear magnetic resonance spectroscopic characterization. Pharm Res. 1993 Feb;10(2):208–13.

31. Angiolini L, Agnes M, Cohen B, Yannakopoulou K, Douhal A. Formation, characterization and pH dependence of rifampicin: heptakis(2,6-di- O -methyl)-β-cyclodextrin complexes. Int J Pharm. 2017 Oct;531(2):668–675.

32. Iza N, Guerrero-Martínez A, Tardajos G, Ortiz MJ, Palao E, Montoro T, et al. Using Inclusion Complexes with Cyclodextrins To Explore the Aggregation Behavior of a Ruthenium Metallosurfactant. Langmuir. 2015 Mar;31(9):2677–2688.

33. Szoka F, Papahadjopoulos D. Comparative Properties and Methods of Preparation of Lipid Vesicles (Liposomes). Annu Rev Biophys Bioeng. 1980 Jun;9(1):467–508.

34. Stewart JCM. Colorimetric determination of phospholipids with ammonium ferrothiocyanate. Anal Biochem. 1980 May;104(1):10–14.

35. Zhang J, Ma PX. Cyclodextrin-based supramolecular systems for drug delivery: Recent progress and future perspective. Adv Drug Deliv Rev. 2013 Aug;65(9):1215–1233.

36. Hudzicki J. Kirby-Bauer Disk Diffusion Susceptibility Test Protocol. Am Soc Microbiol. 2009 Dec;1–23.

37. Zhang H-M, Li Z, Uematsu K, Kobayashi T, Horikoshi K. Antibacterial activity of cyclodextrins against Bacillus strains. Arch Microbiol. 2008 Nov;190(5):605–609.

38. Sohlenkamp C, Geiger O. Bacterial membrane lipids: diversity in structures and pathways. Narberhaus F, editor. FEMS Microbiol Rev. 2016 Jan;40(1):133–159.

39. Furse S, Scott DJ. Three-Dimensional Distribution of Phospholipids in Gram Negative Bacteria. Biochemistry. 2016 Aug;55(34):4742–4747.

40. Bouchet AM, Frías MA, Lairion F, Martini F, Almaleck H, Gordillo G, et al. Structural and dynamical surface properties of phosphatidylethanolamine containing membranes. Biochim Biophys Acta BBA - Biomembr. 2009 May 1;1788(5):918–25.

41. Yesylevskyy SO, Rivel T, Ramseyer C. The influence of curvature on the properties of the plasma membrane. Insights from atomistic molecular dynamics simulations. Sci Rep. 2017 Dec;7(1):16078.

42. Marsh D. Lateral pressure in membranes. Biochim Biophys Acta. 1996 Oct;1286(3):183–223.

43. Clifton LA, Skoda MWA, Daulton EL, Hughes AV, Le Brun AP, Lakey JH, et al. Asymmetric phospholipid: lipopolysaccharide bilayers; a Gram-negative bacterial outer membrane mimic. J R Soc Interface. 2013 Dec 6;10(89):20130810.

44. Clifton LukeA, Ciesielski F, Skoda MWA, Paracini N, Holt SA, Lakey JH. The Effect of Lipopolysaccharide Core Oligosaccharide Size on the Electrostatic Binding of Antimicrobial Proteins to Models of the Gram Negative Bacterial Outer Membrane. Langmuir. 2016 Apr;32(14):3485–3494.

45. Hughes AV. RasCAL download | SourceForge.net [Internet]. 2013 [cited 2018 Oct 7]. Available from: https://sourceforge.net/projects/rscl/

46. Born M, Wolf Emil. Principles of optics : electromagnetic theory of propagation, interference and diffraction of light. Cambridge University Press; 1999. 952 p.

47. Clifton LA, Holt SA, Hughes AV, Daulton EL, Arunmanee W, Heinrich F, et al. An Accurate In Vitro Model of the E. coli Envelope. Angew Chem Int Ed. 2015 Oct;54(41):11952–11955.

48. Haario H, Laine M, Mira A, Saksman E. DRAM: Efficient adaptive MCMC. Stat Comput. 2006 Dec;16(4):339–354.

49. Clifton LA, Skoda MWA, Le Brun AP, Ciesielski F, Kuzmenko I, Holt SA, et al. Effect of Divalent Cation Removal on the Structure of Gram-Negative Bacterial Outer Membrane Models. Langmuir. 2015 Jan;31(1):404–412.

50. Wang J, Matayoshi E. Solubility at the molecular level: development of a critical aggregation concentration (CAC) assay for estimating compound monomer solubility. Pharm Res. 2012 Jul;29(7):1745–54.

51. Drulis-Kawa Z, Gubernator J, Dorotkiewicz-Jach A, Doroszkiewicz W, Kozubek A. A comparison of the in vitro antimicrobial activity of liposomes containing meropenem and gentamicin. Cell Mol Biol Lett. 2006;11(3):360–375.

52. Tandrup Schmidt S, Foged C, Smith Korsholm K, Rades T, Christensen D. Liposome-Based Adjuvants for Subunit Vaccines: Formulation Strategies for Subunit Antigens and Immunostimulators. Pharmaceutics. 2016 Mar;8(1):7.

53. Campbell EA, Korzheva N, Mustaev A, Murakami K, Nair S, Goldfarb A, et al. Structural Mechanism for Rifampicin Inhibition of Bacterial RNA Polymerase. Cell. 2001 Mar 23;104(6):901–12.

54. Miller SI. Antibiotic Resistance and Regulation of the Gram-Negative Bacterial Outer Membrane Barrier by Host Innate Immune Molecules. mBio [Internet]. 2016 Nov 2 [cited 2020 Jan 9];7(5).

55. Clifton LA, Neylon C, Lakey JH. Examining Protein–Lipid Complexes Using Neutron Scattering. In: Methods in molecular biology. 2013. p. 119–150.

56. Uhríková D, Kučerka N, Teixeira J, Gordeliy V, Balgavý P. Structural changes in dipalmitoylphosphatidylcholine bilayer promoted by Ca2+ ions: a small-angle neutron scattering study. Chem Phys Lipids. 2008 Oct;155(2):80–89.

57. Balgavý P, Dubničková M, Kučerka N, Kiselev MA, Yaradaikin SP, Uhríková D. Bilayer thickness and lipid interface area in unilamellar extruded 1,2-diacylphosphatidylcholine liposomes: a small-angle neutron scattering study. Biochim Biophys Acta BBA - Biomembr. 2001 May 2;1512(1):40–52.

58. Antonow D, Thurston DE. Synthesis of DNA-Interactive Pyrrolo[2,1-c][1,4]benzodiazepines (PBDs). Chem Rev. 2011 Apr 13;111(4):2815–64.

59. Bulbake U, Doppalapudi S, Kommineni N, Khan W. Liposomal Formulations in Clinical Use: An Updated Review. Pharmaceutics. 2017 Jun;9(2):12.

60. Deygen IM, Egorov AM, Kudryashova EV. Structure and stability of fluoroquinolone-(2-hydroxypropyl)-β-cyclodextrin complexes as perspective antituberculosis drugs. Mosc Univ Chem Bull. 2016 Jan;71(1):1–6.

61. Chadha R, Saini A, Gupta S, Arora P, Thakur D, Jain DVS. Encapsulation of rifampicin by natural and modified β-cyclodextrins: characterization and thermodynamic parameters. J Incl Phenom Macrocycl Chem. 2010 Jun;67(1–2):109–116.

62. Athanassiou G, Michaleas S, Lada-Chitiroglou E, Tsitsa T, Antoniadou-Vyza E. Antimicrobial activity of β-lactam antibiotics against clinical pathogens after molecular inclusion in several cyclodextrins. A novel approach to bacterial resistance. J Pharm Pharmacol. 2003 Mar;55(3):291–300.

63. Suárez DF, Consuegra J, Trajano VC, Gontijo SML, Guimarães PPG, Cortés ME, et al. Structural and thermodynamic characterization of doxycycline/β-cyclodextrin supramolecular complex and its bacterial membrane interactions. Colloids Surf B Biointerfaces. 2014 Jun;118:194–201.

64. Rosa Teixeira KI, Araújo PV, Almeida Neves BR, Bohorquez Mahecha GA, Sinisterra RD, Cortés ME. Ultrastructural changes in bacterial membranes induced by nano-assemblies β-cyclodextrin chlorhexidine: SEM, AFM, and TEM evaluation. Pharm Dev Technol. 2013 Jun;18(3):600–608.

65. Chen J, Lu W-L, Gu W, Lu S-S, Chen Z-P, Cai B-C, et al. Drug-in-cyclodextrin-in-liposomes: a promising delivery system for hydrophobic drugs. Expert Opin Drug Deliv. 2014 Apr 1;11(4):565–77.

66. Pinheiro M, Pisco S, Silva AS, Nunes C, Reis S. Evaluation of the effect of rifampicin on the biophysical properties of the membranes: Significance for therapeutic and side effects. Int J Pharm. 2014 May;466(1–2):190–197.

67. Huang Z, London E. Effect of Cyclodextrin and Membrane Lipid Structure upon Cyclodextrin–Lipid Interaction. Langmuir. 2013 Nov;29(47):14631–14638.

68. Nishijo J, Moriyama S, Shiota S. Interactions of cholesterol with cyclodextrins in aqueous solution. Chem Pharm Bull (Tokyo). 2003 Nov;51(11):1253–1257.

FOR TABLE OF CONTENTS USE ONLY

Antibiotic-in-cyclodextrin-in-liposomes: formulation development and interactions with model bacterial membranes

Kalliopi-Kelli A. Vandera [($)], Pietro Picconi [($)], Margarita Valero [(&)], Gustavo González-Gaitano [(#)], Arcadia Woods [($)], Luke A. Clifton [(+)], Maximilian W. A. Skoda [(+)], Khondaker Miraz Rahman [($)], Richard D. Harvey [(¥)]*, Cécile A. Dreiss [($)]*

($) School of Cancer & Pharmaceutical Science, Institute of Pharmaceutical Science, King's College London, Franklin-Wilkins Building, 150 Stamford Street, London, SE1 9NH, UK

(&) Department of Physical Chemistry, University of Salamanca, ES E-37007, Salamanca, Spain

(#) Department of Chemistry, University of Navarra, 31080, Pamplona, Spain

(+) Rutherford Appleton Laboratory, ISIS, 1-27, R3, Harwell Campus, Didcot, UK OX11 0QX

(¥) Department of Pharmaceutical Chemistry, University of Vienna, Althanstraße 14, Vienna, Austria

Graphic Abstract